R. & M. No. 3298

MINISTRY OF AVIATION

AERONAUTICAL RESEARCH COUNCIL
REPORTS AND MEMORANDA

Calculation of Stability Derivatives for Tapered Wings of Hexagonal Planform Oscillating in a Supersonic Stream

By DORIS E. LEHRIAN, B.Sc.,
OF THE AERODYNAMICS DIVISION, N.P.L.

LONDON: HER MAJESTY'S STATIONERY OFFICE
1963
PRICE: 18s. 6d. NET

Calculation of Stability Derivatives for Tapered Wings of Hexagonal Planform Oscillating in a Supersonic Stream

By DORIS E. LEHRIAN, B.Sc.,
OF THE AERODYNAMICS DIVISION, N.P.L.

*Reports and Memoranda No. 3298**
September, 1960

Summary.

The aerodynamic loading is formulated for a family of symmetrically tapered wings describing simple harmonic pitching oscillations of low frequency in supersonic flow. The planforms have supersonic leading and trailing edges of constant sweep, the variable parameters being the angle of rake of the side edges and the ratio of span to root chord.

For Mach numbers $\sqrt{2} \leqslant M \leqslant 2{\cdot}4$, the investigation covers supersonic and subsonic side edges which act as leading edges, streamwise tips or trailing edges. The lift and moment are evaluated to first order in frequency on the basis of linearized thin-wing theory. In the case of subsonic trailing side edges, it is more convenient to obtain the total forces by use of the reverse-flow theorem.

The theoretical values of the pitching-moment derivatives are compared with experimental results obtained on half-wing models with alternative pitching axes and a basic 5% double-wedge section. An estimate of thickness effect is calculated by applying two-dimensional aerofoil theory on a strip-theory basis. When corrected for thickness the theoretical values are in good agreement with the experimental derivatives for Mach numbers greater than $1{\cdot}6$.

1. *Introduction.*

The aerodynamic forces acting on oscillating hexagonal wings in a uniform supersonic airstream are to be determined for comparison with experiment. On the basis of linearized theory[1, 2], a formal solution for the perturbation velocity potential on a wing of arbitrary planform and zero thickness is known for simple harmonic oscillations of small amplitude and general frequency. To evaluate the integral for the velocity potential, it is necessary to impose restrictions either on the frequency of oscillation, on the planform of the wing or on the Mach number of the airstream. Since the experiments gave only low frequency, this will be assumed sufficiently small for the neglect of second-order effects. Then, for certain types of planform, an exact solution can be obtained for the velocity potential and hence for the lift distribution.

* Previously issued as A.R.C. 22,186. Published with the permission of the Director, National Physical Laboratory.

The planforms to be considered have symmetrical taper and supersonic leading and trailing edges of 15° sweep. Each wing has a different aspect ratio and side edges which are raked at a varying angle ψ as shown in Figs. 1 and 2. The side edges act as the outboard part of the leading edge if $\psi > 0$, or the trailing edge if $\psi < 0$, and they will be supersonic or subsonic according as M is greater or less than cosec $|\psi|$.

The velocity potential over that part of a polygonal planform which is influenced only by supersonic edges, is defined directly in terms of the upwash field on the planform, and can readily be evaluated. For the tip region of a planform, influenced by a subsonic leading side edge, Evvard[3] uses an equivalent-area concept to simplify the velocity-potential integral for steady flow. For oscillatory motion, Stewartson[2] derives a direct integral for the velocity potential in the tip region; to first order in frequency this integral depends only on the known upwash over Evvard's equivalent area of the planform. This analytical treatment can be extended to cases when the two tip regions overlap, provided that their upwash fields off the planform are independent. Formulae for the velocity-potential distribution over wings with subsonic leading side edges are evaluated analytically for low-frequency pitching oscillations in Section 3. The total lift and pitching moment for a particular planform and Mach number are then obtained by integrating the appropriate formulae over the wing area.

A subsonic trailing side edge greatly complicates the solution, even when formulated in terms of the acceleration potential as suggested by Stewartson[2]. For present purposes however it is not essential to know the distribution of lift. By applying the reverse-flow theorem for oscillatory motion[4], the total forces on a wing with subsonic trailing side edges can be determined from solutions for the same planform when the direction of flow is reversed but the Mach number and frequency of oscillation are unchanged. The application of the reverse-flow theorem for low-frequency pitching oscillations is considered in Section 4.

The stability derivatives are evaluated for eleven planforms and the range of Mach number $\sqrt{2} \leqslant M \leqslant 2 \cdot 4$. For each planform, measured values of the pitching-moment derivatives have been obtained for two or three axis positions from low-frequency tests made on half-wing models at the N.P.L.[6]. These models have a basic 5% double-wedge section, and it may be assumed that the effects of thickness are additive to those of planform, provided that the aspect ratio is not too small. An estimate of the thickness correction is therefore obtained by applying Van Dyke's[5] two-dimensional theory of oscillating aerofoils on a strip-theory basis (Appendix D).

Additional values of the pitching derivatives are calculated for the wing of greatest span with streamwise tips at Mach numbers $1 \cdot 035 \leqslant M \leqslant \sqrt{2}$. This planform was chosen for further investigation to provide some results by linearized theory for comparison with transonic tests which are being made at the N.P.L. For $M = 1 \cdot 035$ the leading and trailing edges of this planform are sonic and the solution is obtained by considering the limiting form of the velocity-potential distributions when $\sigma = \beta \tan \lambda \to 1$.

2. *General Theory.*

2.1. *Linearized Equations.*

In formulating the basic equations of flow it is supposed that an infinitely thin wing of arbitrary planform describes simple harmonic oscillations of small amplitude about zero mean incidence in an otherwise uniform ideal fluid. Effects of wing thickness and viscosity are thus ignored, and squares of perturbations from the uniform supersonic free-stream velocity are neglected throughout the field of flow. The perturbation $\Phi(x, y, z, t)$ in velocity potential then satisfies the linear differential equation (Ref. 1, Table 1)

$$(M^2-1)\frac{\partial^2\Phi}{\partial x^2} - \frac{\partial^2\Phi}{\partial y^2} - \frac{\partial^2\Phi}{\partial z^2} + \frac{2M^2}{U_\infty}\frac{\partial^2\Phi}{\partial x\partial t} + \frac{M^2}{U_\infty{}^2}\frac{\partial^2\Phi}{\partial t^2} = 0\,; \tag{1}$$

the pressure at any point is given by

$$p - p_\infty = -\rho_\infty\left(\frac{\partial\Phi}{\partial t} + U_\infty\frac{\partial\Phi}{\partial x}\right), \tag{2}$$

where U_∞, p_∞ and ρ_∞ are respectively the velocity, pressure and density of the free stream.

The vertical upward displacement of the wing from a mean position $z = 0$ is

$$z(x, y, t) = z_0(x, y)e^{i\omega t} \tag{3}$$

where $z_0(x, y)$ is an arbitrary mode of oscillation to which there corresponds a perturbation potential of complex amplitude

$$\phi(x, y, z) = \Phi(x, y, z, t)e^{-i\omega t}. \tag{4}$$

The linearized boundary condition for tangential flow over the wing is that the amplitude of the upwash

$$w = (\partial\phi/\partial z)_{z=0} = i\omega z_0 + U_\infty(\partial z_0/\partial x). \tag{5}$$

In the wake

$$[i\omega\phi + U_\infty(\partial\phi/\partial x)]_{z=0} = 0\,; \tag{6}$$

by eqn. (2) this ensures that the pressure is continuous across the wake. Since ϕ is antisymmetrical with respect to the plane $z = 0$, $\phi(x, y, +0) = -\phi(x, y, -0)$, and it follows from eqn. (2) that the lift distribution on the wing is

$$l(x, y, t) = 2\rho_\infty[i\omega + U_\infty(\partial/\partial x)]\,[\phi(x, y, +0)]e^{i\omega t}. \tag{7}$$

The problem is therefore to solve eqns. (1), (4), (5) and (6) for $\phi(x, y, +0)$.

2.2. *Integral for the Velocity Potential.*

The various formal solutions for the velocity potential on the upper surface of the wing (e.g., Refs. 1, 2, 3), lead to the integral expression

$$\phi(x, y) = -\frac{1}{\pi}\iint_\Delta w(x', y')K\,dx'dy' \tag{8}$$

in the present notation. Here

$$w(x', y') = [\partial\phi(x', y', z)/\partial z]_{z=0}, \tag{9}$$

$$K = \frac{1}{r}\exp\left[\frac{-i\omega M^2(x-x')}{(M^2-1)U_\infty}\right]\cos\left[\frac{\omega Mr}{(M^2-1)U_\infty}\right] \tag{10}$$

with

$$r = [(x-x')^2 - (M^2-1)(y-y')^2]^{1/2},$$

and the area of integration Δ is the part of the plane $z = 0$ bounded by the forward Mach cone from (x, y) and the wave front defined as the envelope of trailing Mach cones with vertices on the leading edge of the wing. When the wing has only supersonic edges and Δ lies within the planform, eqn. (8) is explicit, since the upwash $w(x', y')$ is known in terms of the wing motion by eqn. (5). If Δ includes any subsonic edges of the wing, $w(x', y')$ is initially unknown over the part of Δ which lies off the planform and has to be evaluated to satisfy (9) before $\phi(x, y)$ can be determined from eqn. (8). The precise treatment will depend on whether the subsonic edges in question are leading or trailing edges.

2.3. *Family of Wings.*

The wings to be considered are symmetrically tapered with side edges inclined at an angle ψ to the direction of the free stream. A typical planform is defined by the apex angle 2λ, the root chord c_0 and the semi-spans s_L and s_T of the leading and trailing edges (Fig. 1). When the side edges are raked outwards, $s_L < s_T = s$ and $\psi > 0$: when they are raked inwards, $s_T < s_L = s$ and $\psi < 0$. The particular planforms for the family of wings are given in terms of λ ($= 75°$), s/c_0 and ψ in Fig. 2.

In a free stream of Mach number $M > \operatorname{cosec} \lambda$, the leading and trailing edges of these wings are supersonic. Any wing of the family associated with a particular Mach number $M = \operatorname{cosec} \mu$ can be classified according to the type of side edge into one of the following five cases:

Case	Semi-span	Range of ψ	Side edges act as
(i)	$s_T < s_L = s$	$\psi \leqslant -\mu$	supersonic (sonic) trailing edge
(ii)	$s_T < s_L = s$	$-\mu < \psi < 0$	subsonic trailing edge
(iii)	$s_L = s_T = s$	$\psi = 0$	streamwise tips
(iv)	$s_L < s_T = s$	$0 < \psi < \mu$	subsonic leading edge
(v)	$s_L < s_T = s$	$\mu \leqslant \psi$	supersonic (sonic) leading edge

On any of these wing planforms consider the region S_0 which lies upstream of the Mach lines from the points $y = \pm s_L$ on the leading edge. For all cases (i) to (v), the velocity potential ϕ at any point in region S_0 is determined by eqns. (5) and (8), where the area of integration $\Delta = \Delta_0$ is bounded by the supersonic leading edge $x = |y| \cot \lambda$ and the forward Mach lines from the point. In case (i) the region S_0 is identical with the planform. In all other cases the velocity potential is required outside the region S_0, over the region of the planform where

$$x > [s_L \cot \lambda + (s_L - |y|) \cot \mu] \tag{11}$$

and $\phi(x, y)$ is influenced by the side edges. Case (iii) with $\psi = 0$ can be regarded as a particular example of case (iv), and both cases are considered in Section 2.4: case (ii) is discussed in Section 2.5. In case (v), where the planform has supersonic leading side edges, eqn. (8) can be applied directly but the area of integration Δ is more complicated than Δ_0: an alternative approach by means of the reverse-flow theorem is therefore adopted in Section 4.

2.4. *Subsonic Leading Side Edges.*

Over that part of the planform covered by (11), the velocity potential in cases (iii) and (iv) is influenced by the upwash field between the leading side edges and the wave front. Furthermore, as shown in Fig. 3, $\phi(x, y)$ in region S_1 or S_2 is influenced by only one side edge, whereas in region

S_3 there is a contribution from both side edges. Region S_3 occurs when the Mach lines from the tips $(s_L \cot \lambda, \pm s_L)$ intersect upstream of the trailing edge, so that eqn. (11) and

$$x > [s_L \cot \lambda + (s_L + |y|) \cot \mu] \tag{12}$$

are both satisfied. The velocity potential over each region S_n is denoted by $(\phi_S)_n$.

By the concept of an equivalent area, Evvard[3] has simplified the integral for $(\phi_S)_n$ in steady flow. Moreover, Stewartson's[2] analytical treatment for general frequencies leads to an integral for $(\phi_S)_n$ which is independent of the upwash field off the planform. These procedures can be applied to $(\phi_S)_3$ over the whole area S_3 provided that the Mach lines from the tips do not intersect the opposite side edges. It follows from Refs. 2 and 3 that the required velocity potentials can be obtained from

$$(\phi_S)_n = -\frac{1}{\pi}\iint_{\Delta_n} w(x', y')K dx' dy' + 0(\omega^2), \tag{13}$$

where K is given in eqn. (10), the areas of integration $\Delta_n (n = 0, 1, 2, 3)$ are defined in Fig. 3, and the upwash $w(x', y')$ is determined by eqn. (5). In the region S_0, the potential $(\phi_S)_0$ follows from eqn. (8) if terms of $0(\omega^2)$ are neglected. To first order in frequency ω, the complete solution for cases (iii) and (iv) can therefore be evaluated from eqn. (13).

2.5. *Subsonic Trailing Side Edges.*

In case (ii), the velocity potential $\phi(x, y)$ over the part of the planform defined by (11) is influenced by the upwash field downstream of the trailing side edges and the wave front. To determine $\phi(x, y)$ from eqn. (8), the upwash $w(x', y')$ must first be evaluated over the part of Δ which lies off the planform; it is difficult to estimate the contribution from the wake and to satisfy the wake condition (6). Stewartson's[2] alternative approach in terms of the acceleration potential yields a convenient integral expression for the lift distribution $l(x, y, t)$ over S_1 and S_2, the regions of the planform influenced by one subsonic trailing edge. The effect of both side edges over the region S_3 defined by (12) would lead to a more complicated expression. Accordingly, no attempt is made to derive the distribution of lift in case (ii). For the limited purpose of obtaining the total forces on a wing, the reverse-flow theorem will be applied (Section 4). Case (ii) is thereby reduced to a problem for a wing with subsonic leading side edges which can be treated by the principles of Section 2.4.

3. *Pitching Solutions for Cases (i), (iii) and (iv).*

3.1. *Functions for the Velocity Potential.*

It follows from Section 2 that, in cases (i), (iii) and (iv), $\phi(x, y)$ to first order in frequency can be expressed directly in terms of the upwash $w(x, y)$ on the planform. For pitching oscillations of amplitude θ_0 about the axis $x = 0$, the wing motion in eqn. (3) is

$$z_0 = -x\theta_0.$$

Then by (5), the upwash distribution is

$$w = -U_\infty[1 + i\nu_0 x/c_0]\theta_0, \tag{14}$$

where the frequency parameter $\nu_0 = \omega c_0/U_\infty$. By taking eqns. (10) and (13) to first order in ν_0, the corresponding velocity potential is

$$\phi(x, y) = \frac{U_\infty \theta_0}{\pi}\iint_{\Delta_n} \frac{1}{r}\left[1 + i\nu_0\left\{\frac{x'}{c_0} - \frac{M^2(x-x')}{c_0(M^2-1)}\right\}\right] dx' dy', \tag{15}$$

where the area of integration Δ_n is defined in Fig. 3 for a point $\mathrm{P} = (x, y)$ in each region S_n of the planform. For pitching motion it is only necessary to determine $\phi(x, y)$ over the regions S_0, S_1 and S_3 of the half-wing.

It is convenient to transform to non-dimensional co-ordinates (X, Y) such that

$$\left.\begin{aligned} x &= c_0 X \sqrt{(M^2-1)} \\ y &= c_0 Y \end{aligned}\right\} ; \tag{16}$$

then all Mach lines in the (X, Y) plane correspond to constant values of $(X \pm Y)$. In these co-ordinates the leading, side and trailing edges of the planforms shown in Figs. 1 and 2 become respectively

$$\left.\begin{aligned} X &= X_L(Y) = \frac{1}{\sigma}\,|Y| && \text{for } 0 \leqslant |Y| \leqslant Y_L \\ X &= X_S(Y) = \frac{1}{\tau}\,|Y| + \left(\frac{1}{\sigma} - \frac{1}{\tau}\right) Y_L && \text{for } |Y| \text{ between } Y_L \text{ and } Y_T \\ X &= X_T(Y) = \frac{1}{\beta} - \frac{1}{\sigma}\,|Y| && \text{for } 0 \leqslant |Y| \leqslant Y_T \end{aligned}\right\} , \tag{17}$$

where

$$\left.\begin{aligned} \beta &= \cot\mu = \sqrt{(M^2-1)} \\ \sigma &= \beta \tan\lambda \geqslant \\ \tau &= \beta \tan\psi \\ Y_L &= s_L/c_0 \\ Y_T &= s_T/c_0 \end{aligned}\right\} \tag{18}$$

and

$$\frac{1}{\sigma}(Y_L + Y_T) + \frac{1}{\tau}(Y_T - Y_L) = \frac{1}{\beta}. \tag{19}$$

Then case (i) is defined by $\tau \leqslant -1$ and $Y_L = s/c_0$; case (iii) by $\tau = 0$ and $Y_L = Y_T = s/c_0$; case (iv) by $0 < \tau < 1$ and $Y_T = s/c_0$. Typical planforms and Mach lines for cases (i) and (iv) are shown in Figs. 4a and 4b respectively. A limitation on Mach number is imposed in cases (iii) and (iv) by the condition that the Mach lines from the tips $(Y_L/\sigma, \pm Y_L)$ do not intersect the opposite side edges, so that

$$\beta(Y_L + Y_T)(\sigma + 1) \geqslant \sigma .$$

In terms of the parameters $Y_T = s/c_0$, λ and ψ which define the planform in cases (iii) and (iv), this condition becomes

$$(M^2-1)^{1/2} \geqslant (1 - 2Y_T \cot\lambda)/(2Y_T - \tan\psi), \tag{20}$$

which gives $M \geqslant 1{\cdot}208$ for the wing $(s/c_0, \lambda, \psi) = (0{\cdot}625, 75°, 15°)$ and less restrictive limits for the other planforms.

In the non-dimensional co-ordinates the velocity potential in eqn. (15) becomes

$$\phi(X, Y) = \frac{U_\infty c_0 \theta_0}{\pi} \iint_{\Delta_n} \frac{1}{R}\left[1 + \frac{i\nu_0}{\beta}\{(1+2\beta^2)X' - (1+\beta^2)X\}\right] dX'dY', \tag{21}$$

where

$$R = [(X-X')^2 - (Y-Y')^2]^{1/2}$$

and Δ_n is now the transformed area of integration when (X, Y) is in the transformed region $\mathrm{S}_n(n = 0, 1, 3)$ of the half-wing. When the leading edge is supersonic $(\sigma > 1)$ and has a kink at the origin, the limits of integration in eqn. (21) will vary within each region S_n. In case (i) where only S_0 occurs, the half-wing subdivides into regions A and B in the (X, Y) plane as can be seen from Fig. 4a for the wing $(s/c_0, \lambda, \psi) = (1\cdot 37, 75°, -45°)$ at $M = 1\cdot 6$. In cases (iii) and (iv) all the regions S_0, S_1, S_3 may occur; in the most complicated example to be considered when $(s/c_0, \lambda, \psi) = (0\cdot 625, 75°, 15°)$ at $M = \sqrt{2}$, Fig. 4b shows seven distinct regions as follows:

$$\left.\begin{array}{l} S_0 \text{ subdivides to give A + B} \\ S_1 \text{ subdivides to give C + D + F} \\ S_3 \text{ subdivides to give E + G} \end{array}\right\} ; \tag{22}$$

of the corresponding areas of integration in the (X, Y) plane, Δ_A and Δ_B are the same as in Fig. 4a and Δ_J for J = C, D, E, F, G, are defined in Fig. 5. At lower Mach numbers consistent with eqn. (20), it is possible to have a further subdivision of S_3, namely J = H, which extends downstream of region G to the kink at the trailing edge. For (X, Y) in region H, the correct application of the equivalent area concept (Section 2.4) gives the area of integration shown in Fig. 5 where the forward part of Δ_H, which is shaded black, must be taken as a negative area of integration.

In terms of the general function

$$F_{mJ}(X, Y) = -\frac{1}{\pi}\iint_{\Delta_J} \frac{1}{R}(X')^m dX'dY', \tag{23}$$

where Δ_J is the area of integration corresponding to any region J = A, B . . . H, eqn. (21) may be written as

$$\phi(X, Y) = -U_\infty c_0 \theta_0 \left[\left\{1 - \frac{i\nu_0(1+\beta^2)X}{\beta}\right\} F_{0J} + i\nu_0 \left\{\frac{1+2\beta^2}{\beta}\right\} F_{1J}\right]. \tag{24}$$

It should be noted that the velocity potential $\phi = U_\infty c_0 F_{mJ}$ corresponds to the upwash distribution $w = U_\infty X^m$ in steady motion. Analytical expressions for F_{mJ} are derived in Appendix A. Formulae for F_{mJ}(J = A, B . . . H and $m = 0, 1$) are given in Appendix B in terms of the non-dimensional co-ordinates (X, Y) and the planform parameters $\sigma > 1$, Y_L and τ. The velocity potential distribution $\phi(X, Y)$ can be determined for any case (i), (iii) and (iv), by eqn. (24) and the appropriate functions F_{mJ}.

On a planform with sonic leading edge $[\sigma = 1]$ and subsonic leading side edges which do not interact $[2\beta(Y_L + Y_T) \geqslant 1]$, the regions J = A, C, D, E and G do not occur and the distinct regions which can arise are

$$S_0 = B, \quad S_1 = F, \quad S_3 = H.$$

The planform $(s/c_0, \lambda, \psi) = (1\cdot 37, 75°, 0)$ at $M = 1\cdot 035$ is shown in Fig. 4c as an example of case (iii) when regions B, F, H occur. When $\sigma = 1$, the velocity potential distribution is given by equation (24) and the limiting form of the functions F_{mJ}. The functions F_{mJ}(J = B, F, H and $m = 0, 1, 2$) can be derived from the formulae in Appendix B by suitably expanding all the $\cos^{-1}$ terms as power series in $(\sigma^2 - 1)^{1/2}$ and taking the limit of F_{mJ} as $\sigma \to 1$. However, Appendix C describes a direct and simpler derivation of the formulae for F_{mJ}; these are expressed in terms of the co-ordinates (X, Y) and the planform parameters Y_L and τ.

3.2. *Pitching Derivatives in Terms of F_{mJ}.*

The lift and pitching moment can now be obtained for low frequency $\nu_0 \to 0$ and supersonic free-stream Mach numbers consistent with eqn. (20). The total forces are

$$\left.\begin{aligned} L &= \iint_S l(x, y)dxdy \\ \mathscr{M} &= -\iint_S xl(x, y)dxdy \end{aligned}\right\}, \tag{25}$$

where $l(x, y)$ is given by eqn. (7). If the lift distribution $l = l_J(X, Y)e^{i\omega t}$ over any region J of the half-wing, then it follows from eqns. (7), (16) and (24) that to first order in ν_0

$$l_J = -2\rho_\infty U_\infty{}^2\theta_0\left[\frac{1}{\beta}F'_{0J} + \frac{i\nu_0}{\beta^2}\{(1+2\beta^2)F'_{1J} - (1+\beta^2)XF'_{0J} - F_{0J}\}\right], \tag{26}$$

where $F'_{mJ} = \partial F_{mJ}/\partial X$. Thus eqn. (25) can be written as

$$\left.\begin{aligned} L &= 2\beta c_0{}^2e^{i\omega t}\sum_J \iint_J l_J dX\,dY \\ \mathscr{M} &= -2\beta^2 c_0{}^3 e^{i\omega t}\sum_J \iint_J Xl_J dX\,dY \end{aligned}\right\}, \tag{27}$$

where the summations extend over all regions J = A, B . . . H which occur within the half-wing.

The aerodynamic derivatives, based on root chord c_0, are now defined by

$$\left.\begin{aligned} L &= \rho_\infty U_\infty{}^2 S\theta_0[l_\theta + i\nu_0 l_{\dot\theta}]e^{i\omega t} \\ \mathscr{M} &= \rho_\infty U_\infty{}^2 Sc_0\theta_0[m_\theta + i\nu_0 m_{\dot\theta}]e^{i\omega t} \end{aligned}\right\} \tag{28}$$

where S = area of the planform. Therefore by eqns. (26) and (27) the aerodynamic derivatives for the pitching axis $h_0 = 0$ in cases (i), (iii) and (iv) are given by

$$\left.\begin{aligned} l_\theta &= -\frac{4c_0{}^2}{S}\sum_J \iint_J F'_{0J}dX\,dY \\ l_{\dot\theta} &= -\frac{4c_0{}^2}{S}\sum_J \iint_J \frac{1}{\beta}\{(1+2\beta^2)F'_{1J} - (1+\beta^2)XF'_{0J} - F_{0J}\}\,dX\,dY \\ m_\theta &= \frac{4c_0{}^2}{S}\sum_J \iint_J \beta XF'_{0J}dX\,dY \\ m_{\dot\theta} &= \frac{4c_0{}^2}{S}\sum_J \iint_J X\{(1+2\beta^2)F'_{1J} - (1+\beta^2)XF'_{0J} - F_{0J}\}\,dX\,dY \end{aligned}\right\}. \tag{29}$$

4. *Pitching Solutions for Cases (ii) and (v).*

4.1. *Statement of the Reverse-Flow Theorem.*

Consider any wing describing simple harmonic oscillations of frequency ω in a uniform supersonic free stream. The reverse-flow theorem is derived by Flax[4] in the form

$$\iint_S l(\xi, \eta, t)\overline{w}_q(\xi, \eta)d\xi\,d\eta = \iint_S \bar{l}_q(\xi, \eta, t)w(\xi, \eta)d\xi\,d\eta, \tag{30}$$

where the integrations over the complete wing area S are referred to co-ordinates (ξ, η) fixed in the wing. Here l and $we^{i\omega t}$ are the lift and upwash distributions over the wing which correspond to a given motion in a direct flow of velocity U_∞; $\bar{l}_q$ and $\bar{w}_q e^{i\omega t}$ are the lift and upwash distributions over the same wing when the motion is arbitrary and the direction of flow is reversed to give a free-stream velocity $-U_\infty$. Eqn. (30) is valid within the limitations imposed by linearized theory and holds for any planform provided that the Kutta condition is satisfied at the trailing edge of the wing for both the direct and the reverse flow.

It is convenient to use the co-ordinates (ξ, η) for the wing describing pitching oscillations in direct flow U_∞, in place of the co-ordinates (x, y) as defined in Fig. 1. Thus for pitching about the axis $\xi = 0$, the upwash distribution is

$$w(\xi, \eta) = -U_\infty[1+i\nu_0\xi/c_0]\theta_0 . \tag{31}$$

For this motion the total lift and pitching moment about $\xi = 0$

$$\left.\begin{aligned} L &= \iint_S l(\xi, \eta, t)d\xi\, d\eta \\ \mathscr{M} &= -\iint_S \xi l(\xi, \eta, t)d\xi\, d\eta \end{aligned}\right\} \tag{32}$$

are required to first order in the frequency parameter $\nu_0 = \omega c_0/U_\infty$. Now if

$$\bar{w}_q(\xi, \eta) = \bar{w}_0 = U_\infty , \tag{33}$$

it follows from eqns. (30) and (32) that the lift can be expressed as

$$L = \iint_S \bar{l}_0(\xi, \eta, t)\frac{w(\xi, \eta)}{U_\infty}d\xi\, d\eta$$

where $\bar{l}_0$ corresponds to $\bar{w}_0$. Then by (31)

$$L = -\theta_0\iint_S \bar{l}_0(\xi, \eta, t)[1 + i\nu_0\xi/c_0]d\xi\, d\eta . \tag{34}$$

Similarly by taking

$$\bar{w}_q(\xi, \eta) = \bar{w}_1 = U_\infty\xi/c_0 , \tag{35}$$

the pitching moment can be expressed as

$$\mathscr{M} = c_0\theta_0\iint_S \bar{l}_1(\xi, \eta, t)[1 + i\nu_0\xi/c_0]d\xi\, d\eta \tag{36}$$

where $\bar{l}_1$ corresponds to $\bar{w}_1$. Hence to determine L and $\mathscr{M}$ for slow pitching oscillations, the lift distributions $\bar{l}_0$ and $\bar{l}_1$ over the wing in reverse flow are required to first order in ν_0.

4.2. *Application of Reverse-Flow Theorem.*

As explained in Sections 2.3 and 2.5, when the side edge acts as a subsonic trailing edge in case (ii) or as a supersonic or sonic leading edge in case (v), no attempt is made to obtain the distribution of lift. The total lift and pitching moment are determined from eqns. (34) and (36) where the solutions $\bar{l}_0(\xi, \eta)$, $\bar{l}_1(\xi, \eta)$ correspond to the respective upwash distributions $\bar{w}_0(\xi, \eta)$, $\bar{w}_1(\xi, \eta)$ defined by eqns. (33) and (35).

In order to obtain the solutions for reverse flow by use of Section 2.4, it is necessary to transform to an equivalent problem of the reversed wing in direct flow, whose co-ordinates are

$$\left.\begin{aligned} x &= c_0 - \xi \\ y &= -\eta \end{aligned}\right\}. \tag{37}$$

The reverse-flow solutions required in cases (ii) and (v) are thus transformed to direct-flow solutions for cases (iv) and (i) respectively. The latter correspond to the upwash distributions

$$\left.\begin{aligned} \bar{w}_0(\xi, \eta) &= w_0(x, y) = U_\infty \\ \bar{w}_1(\xi, \eta) &= w_1(x, y) = U_\infty(c_0 - x)/c_0 \end{aligned}\right\}. \tag{38}$$

Solutions for the corresponding velocity potentials $\phi_q(x, y)$, $(q = 0, 1)$, are derived to first order in frequency by using eqn. (13). The required lift distributions in the (x, y) co-ordinates,

$$\bar{l}_q(\xi, \eta, t) = l_q(x, y, t) \tag{39}$$

can then be determined from eqn. (7).

The derivation of $\phi_q(x, y)$ to first order in ν_0 is similar to the analysis for cases (iv) and (i) in Section 3.1. In the non-dimensional co-ordinates of eqn. (16), $\phi_q(x, y)$ can be expressed as

$$\phi_q(X, Y) = -\frac{U_\infty c_0}{\pi} \iint_{\Delta_n} \frac{1}{R}(1-\beta X')^q \left[1 - \frac{i\nu_0}{\beta}(1+\beta^2)(X-X')\right] dX' dY'. \tag{40}$$

In terms of the general function $F_{mJ}(X, Y)$ defined in (23), eqn. (40) becomes

$$\left.\begin{aligned} \phi_0(X, Y) &= U_\infty c_0 \left[\left\{1 - \frac{i\nu_0(1+\beta^2)X}{\beta}\right\} F_{0J} + i\nu_0 \left\{\frac{1+\beta^2}{\beta}\right\} F_{1J}\right] \\ \phi_1(X, Y) &= \phi_0 - U_\infty c_0[\{\beta - i\nu_0(1+\beta^2)X\}F_{1J} + i\nu_0(1+\beta^2)F_{2J}] \end{aligned}\right\}, \tag{41}$$

where (X, Y) is in any region J $=$ A, B . . . H on the half-planform of the reversed wing. Formulae for $F_{mJ}(X, Y)$ when $\sigma > 1$ are given in Appendix B for $m = 0$, 1 and 2: the parameters σ, Y_L and τ in these formulae now correspond to the semi-apex angle, semi-span of the leading edge, and side-edge angle of the reversed wing. For the particular case $\sigma = 1$, expressions for $F_{mJ}(X, Y)$ are given in Appendix C. Thus ϕ_0 and ϕ_1 can be determined over any reversed planform which classifies as case (iv) or (i) by using eqns. (41) and the appropriate functions F_{mJ}.

4.3. *Pitching Derivatives in Terms of F_{mJ}.*

The lift and pitching moment for low frequency $\nu_0 \to 0$ can now be obtained in cases (ii) and (v) in terms of the lift distributions l_0 and l_1 on the reversed planform. By eqns. (34), (36), (37) and (39)

$$\left.\begin{aligned} L &= -\theta_0 \iint_S l_0(x, y, t)\,[1 + i\nu_0(1 - x/c_0)]\,dx\,dy \\ \mathscr{M} &= c_0\theta_0 \iint_S l_1(x, y, t)\,[1 + i\nu_0(1 - x/c_0)]\,dx\,dy \end{aligned}\right\}, \tag{42}$$

where the integration is over the planform S.

If $l_q(x, y, t) = l_{qJ}(X, Y)e^{i\omega t}$ over any region J of the reversed half-planform, then it follows from eqns. (7), (16) and (41) that to first order in ν_0

$$\left.\begin{aligned} l_{0J} &= 2\rho_\infty U_\infty{}^2\left[\frac{1}{\beta}F'_{0J} + \frac{i\nu_0}{\beta^2}\{(1+\beta^2)F'_{1J} - (1+\beta^2)XF'_{0J} - F_{0J}\}\right] \\ l_{1J} &= l_{0J} - 2\rho_\infty U_\infty{}^2\left[F'_{1J} + \frac{i\nu_0}{\beta}\{(1+\beta^2)F'_{2J} - (1+\beta^2)XF'_{1J} - F_{1J}\}\right] \end{aligned}\right\}, \quad (43)$$

where $F'_{mJ} = \partial F_{mJ}/\partial X$. Thus eqn. (42) can be written as

$$\left.\begin{aligned} L &= -2\beta c_0{}^2\theta_0 e^{i\omega t}\sum_J \iint_J l_{0J}[1 + i\nu_0(1-\beta X)]dX\,dY \\ \mathscr{M} &= 2\beta c_0{}^3\theta_0 e^{i\omega t}\sum_J \iint_J l_{1J}[1 + i\nu_0(1-\beta X)]dX\,dY \end{aligned}\right\}, \quad (44)$$

where the summations extend over all regions J = A, B . . . H which occur within the reversed half-planform, and any terms $0(\nu_0{}^2)$ are to be neglected.

Then by eqns. (28), (43) and (44), the aerodynamic derivatives for the pitching axis $h_0 = 0$ in cases (ii) and (v) are given by

$$\left.\begin{aligned} l_\theta &= -\frac{4c_0{}^2}{S}\sum_J \iint_J F'_{0J}dX\,dY \\ l_{\dot\theta} &= l_\theta - \frac{4c_0{}^2}{S}\sum_J \iint_J \frac{1}{\beta}\{(1+\beta^2)F'_{1J} - (1+2\beta^2)XF'_{0J} - F_{0J}\}dX\,dY \\ m_\theta &= -l_\theta - \frac{4c_0{}^2}{S}\sum_J \iint_J \beta F'_{1J}dX\,dY \\ m_{\dot\theta} &= (m_\theta - l_{\dot\theta} + l_\theta) - \frac{4c_0{}^2}{S}\sum_J \iint_J \{(1+\beta^2)F'_{2J} - (1+2\beta^2)XF'_{1J} - F_{1J}\}dX\,dY \end{aligned}\right\}, \quad (45)$$

where the non-dimensional co-ordinates (X, Y) and the functions F_{mJ} refer to the reversed planform.

5. *Evaluation of Derivatives.*

The derivatives for low-frequency pitching oscillations about the axis $x = h_0c_0 = 0$ have been calculated for eleven wings of the family defined in Figs. 1 and 2. The six Mach numbers $M = \sqrt{2}$, 1·6 (0·2) 2·4 were included for all these planforms, and extra solutions for $M = 2/\sqrt{3} = 1{\cdot}155$ were obtained for the two wings of greatest span with $\psi = 0$ and 45°. Further solutions for the wing ($s/c_0 = 1{\cdot}37$, $\psi = 0$) were evaluated for $M = 1{\cdot}102$, 1·065 and 1·035; these correspond respectively to the following cases:

(*a*) Mach lines from both tips intersecting the trailing edge on the root chord [$\beta s = c_0 - s\cot\lambda$],

(*b*) Mach lines from apex reflected in side edges and intersecting the trailing edge on the root chord [$\beta s = c_0$],

(*c*) Sonic leading and trailing edges [$\beta\tan\lambda = \sigma = 1$].

By the classification defined in Section 2.3 the calculations for each of the wings and Mach numbers are grouped into cases (i) to (v) ,as shown in Table 1.

The derivatives l_θ, $l_{\dot\theta}$, m_θ, $m_{\dot\theta}$ defined in eqn. (28) are evaluated from eqns. (29) in cases (i), (iii) and (iv), and from eqns. (45) in cases (ii) and (v); analytical expressions for the functions F_{mJ} are given in Appendix B for $\sigma > 1$ and in Appendix C for $\sigma = 1$. Since the sweep of the leading and trailing edges remain the same when the planform is reversed, the limits of integration in eqns. (45)

are precisely those for which eqns. (29) are to be evaluated. Moreover, as the integrands have several terms in common, the calculation of the derivatives in case (ii) or (v) is relatively simple once that for the corresponding case (iv) or (i) has been completed. The complexity of the integration depends on the number of regions J which occur on the half planform. In cases (i) and (v) there are only the two regions A and B; the derivatives were evaluated analytically by means of standard integrals and numerical values were then obtained for each particular planform and Mach number by inserting the appropriate limits. If $\sigma > 1$, then in cases (ii), (iii) and (iv) the regions A, B and C always occur, and, as listed in Table 1, one or more of the regions D, E, F and G arise as the aspect ratio and the Mach number decrease. From Appendix B it can be seen that F_{mJ} in regions J $=$ C . . . H are complicated expressions depending on the side-edge parameter $\tau = \beta \tan \psi$. Although the chordwise integration of these formulae was carried out analytically, it was more convenient to evaluate the spanwise integrals numerically for each particular planform and Mach number.

The values of the derivatives l_θ, $l_{\dot{\theta}}$, m_θ, $m_{\dot{\theta}}$ for all combinations of planform and Mach number are presented in Tables 2 to 4 for pitching about the axis $x = 0$. The derivatives for any axis position $x = h_0 c_0$ can then be obtained from the well-known formulae

$$\left.\begin{aligned} l_\theta(h_0) &= l_\theta(0) - h_0 l_z(0) \\ l_{\dot{\theta}}(h_0) &= l_{\dot{\theta}}(0) - h_0 l_{\dot{z}}(0) \\ m_\theta(h_0) &= m_\theta(0) + h_0[l_\theta(0) - m_z(0)] - h_0{}^2 l_z(0) \\ m_{\dot{\theta}}(h_0) &= m_{\dot{\theta}}(0) + h_0[l_{\dot{\theta}}(0) - m_{\dot{z}}(0)] - h_0{}^2 l_{\dot{z}}(0) \end{aligned}\right\}. \tag{46}$$

For low-frequency oscillations $\nu_0 \to 0$, the plunging derivatives are

$$\left.\begin{aligned} l_z(0) &= m_z(0) = 0 \\ l_{\dot{z}}(0) &= l_\theta(0) \\ m_{\dot{z}}(0) &= m_\theta(0) \end{aligned}\right\},$$

and the derivatives in eqn. (46) for a general pitching axis can therefore be evaluated from their tabulated values for $h_0 = 0$.

Since the root chord c_0 is constant for the family of planforms in Fig. 2, the definition of derivatives in eqn. (28) has been used throughout. However, the derivatives are often referred to chord lengths other than c_0: in such cases eqn. (28) would be replaced by

$$\left.\begin{aligned} L &= \rho_\infty U_\infty{}^2 S\theta_0[l_\theta + i\nu l_{\dot{\theta}}]e^{i\omega t} \\ \mathscr{M} &= \rho_\infty U_\infty{}^2 S d\theta_0[m_\theta + i\nu m_{\dot{\theta}}]e^{i\omega t} \end{aligned}\right\}, \tag{47}$$

where $\nu = \omega d/U_\infty$ and d is an arbitrary length. It follows that the derivatives l_θ, $l_{\dot{\theta}}$, m_θ, $m_{\dot{\theta}}$ in eqns. (29) and (45) have to be multiplied by the factors 1, c_0/d, c_0/d, $(c_0/d)^2$ respectively. The geometric (first) mean chord

$$\bar{c} = \int_0^s c(y)dy/s = S/2s, \tag{48}$$

and the aerodynamic (second) mean chord

$$\bar{\bar{c}} = \int_0^s c^2(y)dy \bigg/ \int_0^s c(y)dy \tag{49}$$

are frequently chosen as the representative length d. For ease of transformation the values of the factors $c_0/\bar{c}$, $(c_0/\bar{c})^2$, $c_0/\bar{\bar{c}}$, $(c_0/\bar{\bar{c}})^2$ are given in Table 8 for each of the planforms under consideration.

6. *Discussion of Results.*

The stability derivatives for the family of wings in Fig. 2 are presented in Figs. 6 to 16 for various positions of the pitching axis $x = h_0 c_0$ and Mach numbers in the range $\sqrt{2} \leqslant M \leqslant 2\cdot4$; results for lower M are plotted for two wings of largest span. Section 6.1 considers the values of the lift and pitching-moment derivatives obtained by linearized theory and plotted in Figs. 6 to 10 for a selection of the planforms. The theoretical effect of profile shape is discussed in Section 6.2. These results are compared with measured values of the pitching-moment derivatives in Figs. 11 to 16, which are analysed in Section 6.3.

6.1. *Linearized Theory.*

In Fig. 6, values of l_θ are plotted against $[M + s/c_0 + 0\cdot01|\psi|]$ to show the variation with Mach number, wing span and side-edge rake. Since $\nu_0 \to 0$, l_θ is independent of h_0 and by the reverse-flow theorem is shown to be independent of the sign of ψ. Additional values of this derivative were computed for $|\psi| = 15°$ and $|\psi| = \text{cosec}^{-1}M$ to facilitate the drawing of Fig. 6. The curves show that the variation in the planform parameter s/c_0 produces a large change in l_θ when $M = \sqrt{2}$ and progressively smaller changes as M increases up to $2\cdot4$. For constant M and s/c_0, the curves of l_θ show marked discontinuities in slope when the side edges become sonic ($|\psi| = \text{cosec}^{-1}M$). The derivative decreases slightly as $|\psi|$ increases above or decreases below this value; the latter effect becomes more pronounced as the wing span becomes smaller.

For the planform $(s/c_0, \psi) = (1\cdot37, 0)$ in Fig. 7, the lift and moment derivatives for $h_0 = 0$ show large rates of change with M at the lower values of M. The stiffness derivative $-m_\theta$ appears to have a maximum value near $M = 1\cdot064$ and to decrease sharply as M decreases to $1\cdot035$; the damping derivative $-m_{\dot\theta}$ becomes negative for $M < 1\cdot3$. The graphs of Fig. 7 for $M > 1\cdot155$ are typical of all planforms having $s/c_0 = 1\cdot37$, as it can be seen from the values in Table 2 that the effect of ψ is very small. Fig. 8 shows the effect of wing span on the derivatives $l_{\dot\theta}$, $-m_\theta$, $-m_{\dot\theta}$ for the mid-chord pitching axis. The lift derivatives l_θ in Fig. 6 and $l_{\dot\theta}$ in Fig. 8a show the least variation with Mach number ($M > \sqrt{2}$) for the wings of smallest span. There are marked differences in the pitching-moment derivatives for the three spans; unlike that for the lift derivatives, the variation with Mach number in Fig. 8b is most pronounced for the wings of smallest span. The left and right diagrams of Figs. 8a and 8b confirm that the effect of raked trailing edges is small and only becomes important as s/c_0 decreases.

The variation of the damping derivative $-m_{\dot\theta}$ with pitching axis is illustrated in Figs. 9 and 10. On the planforms with streamwise tips at $M = \sqrt{2}$, there is considerable variation with h_0 and with wing span; negative damping is indicated in Fig. 9a on planforms $s/c_0 > 1$ at axis positions in the neighbourhood of $h_0 = 0\cdot35$. When $M = 2$, the effect of aspect ratio is small and there is less variation with h_0 in Fig. 9b. For axis positions forward of mid-chord the increase in M gives greater damping for the two larger planforms with streamwise tips, but a loss in damping for $s/c_0 = 0\cdot625$. Similar effects on a streamwise tip planform and two raked planforms are illustrated in Figs. 10a to 10c by curves for various fixed Mach numbers. The wings of largest span exhibit large negative damping when $M \leqslant 1\cdot155$ for pitching axes forward of the mid-chord; for the wing $(s/c_0, \psi) = (1\cdot37, 0)$ in Fig. 10a, the axis position for zero damping moves from $h_0 = 0\cdot54$ to $0\cdot41$ as M decreases from $1\cdot102$ to $1\cdot035$. The close similarity between the curves for $M = 2\cdot4$ in Figs. 10b and 10c, illustrates the decreasing influence of aspect ratio and side-edge rake at the higher supersonic Mach numbers.

6.2. *Thickness Corrections.*

To extend the usefulness of the comparison of theory and experiment, some allowance is made for the finite thickness of the wings. The half-wing models with streamwise tips had symmetrical double-wedge sections with constant thickness/chord ratio of $0 \cdot 05$. Each model was cropped at the angle ψ to give a blunt raked side edge. In the particular case $(s/c_0, \psi) = (1, \pm 30°)$, the model was later chamfered to give a sharp side edge and a 5% double-wedge streamwise section across the whole span.

Van Dyke's theory[5] for a two-dimensional oscillating aerofoil of small finite thickness is applied to the three-dimensional wings by using simple strip theory. Van Dyke's theory assumes that the aerofoil has a sharp leading edge with attached shock wave. It can therefore be applied to the wings with blunt or sharp trailing side edges and to the wings with streamwise tips. Application to the wings with leading side edges is rather dubious, but it has been used for the chamfered model.

On this approximate basis, the thickness corrections to lift and moment for slow pitching oscillations are formulated in Appendix D. For the particular wings having a 5% thick double-wedge section the incremental corrections to the derivatives are given by eqn. (D.7) with $\delta = 0 \cdot 05$. It can be seen that $\Delta l_\theta = 0$ and that for wings with raked side edges $\Delta l_{\dot\theta}$ and Δm_θ are independent of the sign of ψ.

Values of the thickness corrections Δl_θ, $\Delta l_{\dot\theta}$, Δm_θ, $\Delta m_{\dot\theta}$ are given in Tables 5 to 7 for the eleven wings at the six Mach numbers $M = \sqrt{2}$, $1 \cdot 6$ $(0 \cdot 2)$ $2 \cdot 4$; the values are for wings with either blunt trailing side edges $(\psi < 0)$, streamwise tips $(\psi = 0)$ or sharp leading side edges $(\psi > 0)$ and are referred to the pitching axis $h_0 = 0$. The thickness corrections decrease as the Mach number increases and are small compared with the values of the derivatives given in Tables 2 to 4 for wings of zero thickness. Apart from Δl_θ for blunt trailing side edges, the thickness corrections are practically independent of side-edge angle; similarly $\Delta l_{\dot\theta}$, Δm_θ and $\Delta m_{\dot\theta}$ are hardly affected by chamfering to give a sharp trailing side edge. When the wing is pitching about an arbitrary axis $x = h_0 c_0$, the thickness corrections can be obtained from the transformation formulae in eqn. (46). For all planforms, $- \Delta m_{\dot\theta}$ is negative for $h_0 = 0$, but for axis positions $h_0 > \frac{1}{2}$ the thickness correction to the damping is always positive.

It should be borne in mind that, since the flow over the wings is nowhere two-dimensional, the use of strip theory will lead to error; this applies especially to the region influenced by the wing tips. However, Tables 5 to 7 may be expected to give the sign and order of magnitude of the small corrections for thickness.

6.3. *Comparison with Experiment.*

Pitching-moment derivatives were measured on half-wing models in the N.P.L. 11 in. Supersonic Wind Tunnel for $1 \cdot 38 < M < 2 \cdot 47$ by the free-oscillation technique described in Ref. 6. The oscillations corresponded to low values of the frequency parameter $\nu_0 = \omega c_0/U_\infty < 0 \cdot 03$ and mean amplitude of $\theta_0 \doteqdot 0 \cdot 017$ radians. For some of the tests the value of $- m_{\dot\theta}$ varied with amplitude; the result quoted is the mean value for the whole amplitude range $(0 \cdot 006 < \theta_0 < 0 \cdot 03)$. Planforms having a raked trailing edge $(\psi < 0)$ were tested for the two pitching axes $h_0 = 0 \cdot 4$ and $h_0 = 0 \cdot 5$. By inverting the models, results for raked leading edges $(\psi > 0)$ were obtained for $h_0 = 0 \cdot 5$ and $h_0 = 0 \cdot 6$. The planforms with streamwise tips were oscillated about all three axis positions. A limited comparison of the calculated and measured values of $- m_\theta$ and $- m_{\dot\theta}$ for the eleven wings is made in Figs. 11 to 16.

The variation of the derivatives with Mach number is shown for three wings in Figs. 11 to 13. Each wing has a different span, type of side edge and thickness distribution across the span: the side edges of the two raked wings are supersonic for $M > 2$ and subsonic for $M < 2$. It can be seen from Figs. 11 to 13 that $-m_\theta$ from linearized theory exceeds the measured values for all three wings and each axis position; however, the rates of change of $-m_\theta$ with M are very similar. By allowing for thickness, the agreement between the theoretical and experimental values of $-m_\theta$ is considerably improved. The calculated values of $-m_{\dot\theta}$ for the three wings agree quite well with the measured values when $M > 1 \cdot 8$. At these Mach numbers, the effect of thickness is almost negligible when $h_0 = 0 \cdot 5$, and gives only a slight loss or gain in damping as the pitching axis moves to $h_0 = 0 \cdot 4$ or $h_0 = 0 \cdot 6$ respectively. When $M < 1 \cdot 8$, the thickness correction to $-m_{\dot\theta}$ is very small for $h_0 = 0 \cdot 4$ but increases as the axis moves downstream; the agreement between theory and experiment is significantly improved by allowing for thickness, even though the discrepancies become larger as M decreases to $\sqrt{2}$. It can be seen from Figs. 11 to 13 that the comparison is fairly consistent for all three wings.

The effect of varying the pitching axis $x = h_0 c_0$ of the wing $(s/c_0, \psi) = (1, 0)$ is shown in Figs. 14a and b for Mach numbers $M = \sqrt{2}$ and $M = 2$. Comparison with measured values indicates that the thickness correction improves the calculated values of both $-m_\theta$ and $-m_{\dot\theta}$; the variation with axis position is similar to that measured. For $h_0 < 0 \cdot 37$ it is noted that the thickness correction reduces the calculated value of $-m_{\dot\theta}$ for both $M = \sqrt{2}$ and $M = 2$, and gives some negative damping at the lower Mach number.

In Figs. 15 and 16, the moment derivatives for the mid-chord pitching axis are presented for all the eleven wings to show the effect of raking the side edges when $M = \sqrt{2}$ and $M = 2$ respectively. The thickness corrections given here correspond to a 5% double-wedge section; for $\psi < 0$ these corrections differ only slightly from the values for blunt trailing side edges (*see* Section 6.2). Even at $M = \sqrt{2}$, chamfering the half-wing models had but small effect on the measured pitching moments for the two wings $(s/c_0, \psi) = (1, \pm 30°)$. Both the calculated and measured values of $-m_\theta$ and $-m_{\dot\theta}$ show that side-edge rake has an important effect as the wing span becomes smaller and as the Mach number decreases. The thickness corrections improve the agreement with experiment in all cases except $(s/c_0, \psi) = (0 \cdot 625, \pm 15°)$. For these low aspect ratio wings, the tip effects become more important and thickness corrections based on two-dimensional strip theory are likely to be unreliable especially at low Mach numbers.

7. *Conclusions.*

1. Exact linearized solutions for low-frequency pitching derivatives have been obtained for the combinations of wing planform and Mach number defined in Section 2.3. The methods of solution can be extended to other modes of oscillation and to more general hexagonal planforms. The functions F_{mJ} given in Appendix B can be utilised for any wing having supersonic leading and trailing edges and non-interacting side edges.

2. For the Mach number range $\sqrt{2} \leqslant M \leqslant 2 \cdot 4$, exact linearized theory gives values of the pitching-moment derivatives in qualitative agreement with experiments on eleven planforms; the calculated and measured values indicate the same trends with Mach number and axis position.

3. As described in Appendix D, the effect of small finite thickness on three-dimensional wings can readily be estimated on the basis of two-dimensional strip theory. For the 5% thick double-wedge

section, the thickness corrections are not large but they improve significantly the comparison between theory and experiment. At the lower Mach numbers such thickness corrections should be used with caution when the aspect ratio is small.

8. *Acknowledgement.*

The numerical results given in this report were calculated by Mrs. B. O. Armour of the Aerodynamics Division, N.P.L.

NOTATION

a	Speed of sound at infinity
$c(y)$; c_0	Local wing chord; root chord
$\bar{c}$; $\bar{\bar{c}}$	Geometric mean chord [$= S/2s$]; aerodynamic mean chord [eqn. (49)]
$F_{mJ}(X, Y)$	Function defined by eqn. (23)
F'_{mJ}	$= \partial F_{mJ}/\partial X$
h_0	Values of x/c_0 along pitching axis (Fig. 1)
J	Typical region of planform in (X, Y) plane; J = A, B . . . H (Figs. 4 and 5)
K	Kernel function in integral for $\phi(x, y)$ [eqn. (10)]
$l(x, y, t)$	Lift distribution on the planform
$\bar{l}_q(\xi, \eta, t)$	Lift distribution on a wing in reverse flow [Section 4.1]
$l_q(x, y, t)$	Lift distribution on the reversed planform when $w = w_q(x, y)$
l_θ, $l_{\dot\theta}$	Lift derivatives for pitching oscillations [eqns. (28) and (46)]
L	Lift
m_θ, $m_{\dot\theta}$	Direct pitching derivatives [eqns. (28) and (46)]
M	Mach number [$= U_\infty/a$]
$\mathscr{M}$	Pitching moment about axis $h_0 = 0$
p	Pressure
r	$= [(x-x')^2 - \beta^2(y-y')^2]^{1/2}$
R	$= [(X-X')^2 - (Y-Y')^2]^{1/2}$
s	Semi-span of wing
s_L, s_T	Semi-span of the leading and trailing edges
S	Area of wing planform
S_n	Region of the planform in Fig. 3 ($n = 0, 1, 2, 3$)
t	Time
U_∞	Free-stream velocity
$w(x, y)$	Complex upwash [$= (\partial\phi/\partial z)_{z=0}$]
$\bar{w}_q(\xi, \eta)$	Complex upwash on a wing in reverse flow, $q = 0$ and 1 [Section 4.1]
$w_q(x, y)$	Complex upwash on the reversed planform, defined by eqn. (38) for $q = 0$ and 1
x, y, z	Co-ordinates defined in Fig. 1
$z_0(x, y)$	Mode of oscillation [eqn. (3)]
X, Y	Non-dimensional co-ordinates [$= x/\beta c_0$, y/c_0]
X_L, X_S, X_T	Functions of Y in eqns. (17)
Y_L; Y_T	$= s_L/c_0$; s_T/c_0
β	$= [M^2-1]^{1/2} = \cot\mu$

NOTATION—*continued*

Δ		Area of integration in eqn. (8)
Δ_J	=	Δ for (X, Y) in region J (Figs. 4 and 5)
Δ_n	=	Δ for (x, y) in region S_n (Fig. 3)
θ; θ_0		Angular displacement of wing for pitching oscillations; complex amplitude of θ
λ		Semi-apex angle of wing planform (Fig. 1)
μ		Mach angle [$= \text{cosec}^{-1} M$]
ν_0		Frequency parameter [$= \omega c_0/U_\infty$]
ξ, η		Co-ordinates replacing (x, y) in Section 4.1
ρ_∞		Free-stream density
σ	=	$\beta \tan \lambda$
τ	=	$\beta \tan \psi$
$\phi(x, y)$		Complex amplitude of Φ, on upper surface $z = +0$ of wing
$\phi_q(x, y)$		Distribution of ϕ over the reversed planform when $w = w_q$
$(\phi_S)_n$	=	$\phi(x, y)$ over region S_n
$\Phi(x, y, z, t)$		Perturbation-velocity potential
ψ		Angle of rake of the side edges (of the same sign as $s_T - s_L$)
ω	=	$2\pi \times$ (frequency of oscillation)

REFERENCES

No.	Author	Title, etc.
1	J. W. Miles	*The potential theory of unsteady supersonic flow.* Cambridge University Press. 1959.
2	K. Stewartson	On the linearized potential theory of unsteady supersonic motion. Part II. *Quart. J. Mech. App. Math.* Vol. 5. p. 137. 1952.
3	J. C. Evvard	Use of source distributions for evaluating theoretical aerodynamics of thin finite wings at supersonic speeds. N.A.C.A. Report 951. 1950.
4	A. H. Flax	Reverse-flow and variational theorems for lifting surfaces in non-stationary compressible flow. *J. Ae.Sci.* Vol. 20. p. 120. 1953.
5	M. D. Van Dyke	Supersonic flow past oscillating airfoils including nonlinear thickness effects. N.A.C.A. Report 1183. 1954.
6	L. Woodgate, J. Maybrey and C. Scruton	Measurement of the pitching-moment derivatives for rigid tapered wings of hexagonal planform oscillating in supersonic flow. A.R.C. R. & M. 3294. March, 1961.

APPENDIX A

Evaluation of $F_{mJ}(X, Y)$

The function F_{mJ} defined by eqn. (23) is required for (X, Y) in each region J = A, B . . . H of a planform with supersonic leading edge ($\sigma > 1$) which classifies as case (i), (iii) or (iv). The areas of integration Δ_J are defined in Figs. 4a and 5, and these can be expressed most simply in co-ordinates (u, v) and (u_0, v_0) such that

$$u\sqrt{2} = X' - Y', \quad v\sqrt{2} = X' + Y' \tag{A.1}$$

and

$$u_0\sqrt{2} = X - Y, \quad v_0\sqrt{2} = X + Y. \tag{A.2}$$

By equations (17) and (18), the leading and side edges of the planform are respectively

$$\left.\begin{aligned} u_0 &= \gamma v_0 \quad \text{when } v_0 > u_0 \text{ (positive } Y) \\ v_0 &= \gamma u_0 \quad \text{when } v_0 < u_0 \text{ (negative } Y) \end{aligned}\right\} \tag{A.3}$$

and

$$\left.\begin{aligned} u_0 &= \bar{u}_0 = \delta v_0 - \epsilon Y_L \text{ when } v_0 > u_0 \\ v_0 &= \bar{v}_0 = \delta u_0 - \epsilon Y_L \text{ when } v_0 < u_0 \end{aligned}\right\}, \tag{A.4}$$

where

$$\left.\begin{aligned} \gamma &= (1-\sigma)/(1+\sigma) \\ \delta &= (1-\tau)/(1+\tau) \\ \epsilon &= \frac{(\sigma-\tau)\sqrt{2}}{\sigma(1+\tau)} \end{aligned}\right\}. \tag{A.5}$$

Thus the area of integration Δ_J for any point (u_0, v_0) is defined in the following table:

Region J	Area Δ_J is bounded by $u = u_0$, $v = v_0$ and the lines
A	$u = \gamma v$
B	$u = \gamma v$, $v = \gamma u$
C	$u = \gamma v$, $u = \bar{u}_0$
D	$u = \gamma v$, $v = \gamma u$, $u = \bar{u}_0$
E	$u = \gamma v$, $v = \gamma u$, $u = \bar{u}_0$, $v = \bar{v}_0$
F	$v = \gamma u$, $u = \bar{u}_0$
G	$v = \gamma u$, $u = \bar{u}_0$, $v = \bar{v}_0$
H	$u = \gamma v$, $v = \gamma u$, $u = \bar{u}_0$, $v = \bar{v}_0$

By eqns. (23), (A.1) and (A.2) the integral for F_{mJ} becomes

$$F_{mJ}(u_0, v_0) = \iint_{\Delta_J} f_m(u, v)\,du\,dv, \tag{A.6}$$

where

$$f_m(u, v) = -\frac{1}{\pi\sqrt{2}}\left(\frac{u+v}{\sqrt{2}}\right)^m (u_0-u)^{-1/2}(v_0-v)^{-1/2} \tag{A.7}$$

This is evaluated by considering the following double integrals

$$\left.\begin{aligned} i_m(u_1, v_1) &= \int_{v=0}^{v_1} \int_{u=0}^{u_1} f_m(u, v) du\, dv \\ j_m(u_1, v_1) &= \int_{v=u_1/\gamma}^{v_1} \int_{u=\gamma v}^{u_1} f_m(u, v) du\, dv \\ k_m(u_1, v_1) &= \int_{u=v_1/\gamma}^{u_1} \int_{v=\gamma u}^{v_1} f_m(u, v) dv\, du \end{aligned}\right\}, \tag{A.8}$$

where $u_1 \leqslant u_0$ and $v_1 \leqslant v_0$ are arbitrary limits. By consideration of eqns. (A.4) to (A.8) and the definitions of Δ_J in the above table it follows that

$$\left.\begin{aligned} F_{mA} &= j_m(u_0, v_0) \\ F_{mB} &= i_m(u_0, v_0) + j_m(0, v_0) + k_m(u_0, 0) \\ F_{mC} &= F_{mA}(u_0, v_0) - j_m(\bar{u}_0, v_0) \\ F_{mD} &= F_{mB}(u_0, v_0) - j_m(\bar{u}_0, v_0) \\ F_{mE} &= F_{mD}(u_0, v_0) - k_m(u_0, \bar{v}_0) \\ F_{mF} &= k_m(u_0, v_0) - k_m(\bar{u}_0, v_0) \\ F_{mG} &= F_{mF}(u_0, v_0) - k_m(u_0, \bar{v}_0) \\ F_{mH} &= F_{mF}(u_0, v_0) - F_{mB}(u_0, v_0) + j_m(u_0, v_0) - j_m(u_0, \bar{v}_0) \end{aligned}\right\}. \tag{A.9}$$

The integrals of eqns. (A.7) and (A.8) were evaluated in terms of (u_1, v_1) by standard integration. Each of the functions $F_{mJ}(u_0, v_0)$ for J $=$ A, B . . . H was then derived from eqn. (A.9) by inserting the appropriate values of u_1 and v_1; formulae were obtained for $m = 0$, 1 and 2. By use of eqns. (A.2), (A.4) and (A.5), the formulae for F_{mJ} were expressed in terms of the non-dimensional co-ordinates (X, Y) and the planform parameters σ, Y_L and τ defined in eqns. (18).

APPENDIX B

Formulae for F_{mJ}; J $=$ A, B . . . H, $m = 0, 1, 2$

The formulae presented here apply to planforms with a supersonic leading edge ($0 \leqslant 1/\sigma < 1$) and side edges which act as subsonic leading edges ($0 < \tau < 1$) or as streamwise tips ($\tau = 0$), providing that any region J on the planform is independent of the flow in the wake. The method of evaluation is described in Appendix A: $\zeta = \sigma/(\sigma^2 - 1)^{1/2}$

Region A

$$\left.\begin{aligned} F_{0A} &= -A_1 \\ F_{1A} &= XF_{0A} + \tfrac{1}{2}A_2 \\ F_{2A} &= 2XF_{1A} - X^2F_{0A} - \tfrac{1}{6}\{(2\sigma^2+1)/\sigma^2\}A_3 \end{aligned}\right\},$$

where

$$A_p = \zeta^{2p-1}\left[X - \frac{1}{\sigma}Y\right]^p.$$

Region B

$$\left.\begin{aligned} F_{0B} &= -B_1 \\ F_{1B} &= XF_{0B} + \tfrac{1}{2}B_2 - (\zeta^2/\sigma)XH_1 \\ F_{2B} &= 2XF_{1B} - X^2F_{0B} - \tfrac{1}{6}\{(2\sigma^2+1)/\sigma^2\}B_3 + \Omega_B \end{aligned}\right\},$$

where

$$B_p = \frac{\zeta^{2p-1}}{\pi}\left[\left(X - \frac{1}{\sigma}Y\right)^p \cos^{-1}\left\{\frac{X-\sigma Y}{\sigma X - Y}\right\} + \left(X + \frac{1}{\sigma}Y\right)^p \cos^{-1}\left\{\frac{X+\sigma Y}{\sigma X + Y}\right\}\right]$$

$$H_p = \frac{1}{\pi}[X^2 - Y^2]^{p/2}$$

and

$$\Omega_B = (\zeta^4/3\sigma^3)[(4\sigma^2+2)X^2H_1 - 3H_3].$$

Regions C and D

$$\left.\begin{aligned} &\text{For } (X,\ Y) \text{ in region C, } F_{mC} = F_{mA}(X,\ Y) - P_m \\ &\text{For } (X,\ Y) \text{ in region D, } F_{mD} = F_{mB}(X,\ Y) - P_m \end{aligned}\right\},$$

where

$$\begin{aligned} P_0 &= -C_1 \\ P_1 &= XP_0 + \tfrac{1}{2}C_2 + \{(\sigma-2)/3\sigma\}I_3 \\ P_2 &= 2XP_1 - X^2P_0 - \tfrac{1}{6}\{(2\sigma^2+1)/\sigma^2\}C_3 + \Omega_C. \end{aligned}$$

The functions C_p and I_p are conveniently expressed in terms of $(X_1,\ Y_1)$ where $X_1 = \left(X - \frac{1}{\sigma}Y_L\right)$, $Y_1 = (Y - Y_L)$; then

$$C_p = \zeta^{2p-2}\left[X_1 - \frac{1}{\sigma}Y_1\right]^{p-1} C_1$$

$$C_1 = \frac{\zeta}{\pi}\left(X_1 - \frac{1}{\sigma}Y_1\right)\cos^{-1}\left\{1 - \frac{2(\sigma-\tau)(X_1+Y_1)}{(\tau+1)(\sigma X_1 - Y_1)}\right\} - I_1$$

$$I_p = \frac{2\zeta^p}{\pi}\left[\frac{(\sigma-\tau)(X_1+Y_1)}{\sigma(\tau+1)}\right]^{p/2}\left[\frac{(\sigma+1)(\tau X_1 - Y_1)}{\sigma(\tau+1)}\right]^{1/2}$$

and

$$\Omega_C = \frac{4}{45}\left[2 - \frac{6}{\sigma} + \frac{7}{\sigma^2}\right]I_5 - \frac{\zeta^2}{9}\left[4 - \frac{12}{\sigma} + \frac{5}{\sigma^2}\right]\left[X_1 - \frac{1}{\sigma}Y_1\right]I_3$$

Region F

$$\left.\begin{aligned} F_{0\mathrm{F}} &= -D_1 \\ F_{1\mathrm{F}} &= XF_{0\mathrm{F}} + \tfrac{1}{2}D_2 - \{(\sigma+2)/3\sigma\}J_3 \\ F_{2\mathrm{F}} &= 2XF_{1\mathrm{F}} - X^2F_{0\mathrm{F}} - \tfrac{1}{6}\{(2\sigma^2+1)/\sigma^2\}D_3 - \Omega_{\mathrm{D}} \end{aligned}\right\}.$$

It is convenient to express the functions D_p and J_p in terms of the co-ordinates $(X_2,\ Y_2)$ such that

$$X_2 = X + \frac{1}{\sigma}\left(\frac{\sigma-\tau}{\sigma+\tau}\right) Y_L, \quad Y_2 = Y - \left(\frac{\sigma-\tau}{\sigma+\tau}\right) Y_L;$$

then

$$D_p = \zeta^{2p-2}\left[X_2 + \frac{1}{\sigma}Y_2\right]^{p-1} D_1$$

$$D_1 = \frac{\zeta}{\pi}\left(X_2 + \frac{1}{\sigma}Y_2\right)\left[\pi - \cos^{-1}\left\{1 - \frac{2(\sigma+\tau)(X_2+Y_2)}{(\tau+1)(\sigma X_2+Y_2)}\right\}\right] + J_1$$

$$J_p = \frac{2\zeta^p}{\pi}\left[\frac{(\sigma+\tau)(X_2+Y_2)}{\sigma(\tau+1)}\right]^{p/2}\left[\frac{(\sigma-1)(\tau X_2 - Y_2)}{\sigma(\tau+1)}\right]^{1/2}$$

and

$$\Omega_{\mathrm{D}} = \frac{4}{45}\left[2 + \frac{6}{\sigma} + \frac{7}{\sigma^2}\right] J_5 - \frac{\zeta^2}{9}\left[4 + \frac{12}{\sigma} + \frac{5}{\sigma^2}\right]\left[X_2 + \frac{1}{\sigma}Y_2\right] J_3$$

Regions E and G

$$\left.\begin{aligned} &\text{For } (X,\ Y) \text{ in region E,} \quad F_{m\mathrm{E}} = F_{m\mathrm{D}}(X,\ Y) - Q_m \\ &\text{For } (X,\ Y) \text{ in region G,} \quad F_{m\mathrm{G}} = F_{m\mathrm{F}}(X,\ Y) - Q_m \end{aligned}\right\},$$

where

$$\begin{aligned} Q_0 &= -E_1 \\ Q_1 &= XQ_0 + \tfrac{1}{2}E_2 + \{(\sigma-2)/3\sigma\}K_3 \\ Q_2 &= 2XQ_1 - X^2Q_0 - \tfrac{1}{6}\{(2\sigma^2+1)/\sigma^2\}E_3 + \Omega_{\mathrm{E}}. \end{aligned}$$

It can be shown that

$$\begin{aligned} E_p &= C_p(X_3,\ Y_3) \\ K_p &= I_p(X_3,\ Y_3) \\ \Omega_{\mathrm{E}} &= \Omega_{\mathrm{C}}(X_3,\ Y_3) \end{aligned}$$

where

$$X_3 = \left(X - \frac{1}{\sigma}Y_L\right), \quad Y_3 = -(Y + Y_L).$$

Region H

For $(X,\ Y)$ in region H, it can be shown that

$$F_{m\mathrm{H}} = F_{m\mathrm{F}}(X,\ Y) + F_{m\mathrm{F}}(X - Y) - F_{m\mathrm{B}}(X,\ Y).$$

APPENDIX C

Functions $F_{mJ}(X, Y)$ for Sonic Leading Edge

The function $F_{mJ}(X, Y)$ defined by equation (23) is required for (X, Y) in each region $J = B, F, H$ of a planform with sonic leading edge ($\sigma = 1$) and side edges which act as subsonic leading edges ($0 < \tau < 1$) or streamwise tips ($\tau = 0$).

For the particular case $\sigma = 1$, equations (A.1) to (A.7) of Appendix A apply with $\gamma = 0$. The area of integration Δ_J for a point (u_0, v_0) in region J is defined in the following table.

Region J	Area Δ_J is bounded by $u = u_0$, $v = v_0$ and the lines
B	$u = 0, \quad v = 0$
F	$v = 0, \quad u = \bar{u}_0$
H	$u = \bar{u}_0, \quad v = \bar{v}_0$

The integral for F_{mJ} is given in (u_0, v_0) co-ordinates by equation (A.6); by considering the double integral $i_m(u_1, v_1)$ of equation (A.8) and the above definitions for Δ_J, the functions F_{mJ} can be expressed as

$$F_{mB} = i_m(u_0, v_0)$$

$$F_{mF} = F_{mB}(u_0, v_0) - i_m(\bar{u}_0, v_0)$$

$$F_{mH} = F_{mF}(u_0, v_0) - i_m(u_0, \bar{v}_0)$$

where

$$\bar{u}_0 = \delta(v_0 - \sqrt{2Y_L}),$$

$$\bar{v}_0 = \delta(u_0 - \sqrt{2Y_L}),$$

$$\delta = (1-\tau)/(1+\tau).$$

Expressions for F_{mJ}($J = B, F, H$ and $m = 0, 1, 2$) have been obtained by inserting into the standard integrals $i_m(u_1, v_1)$ the values (u_1, v_1) appropriate to each region J. The resulting formulae for $F_{mJ}(X, Y)$ can be expressed concisely in terms of the following functions $\Psi_m(P, Q)$:

$$\left.\begin{aligned} \Psi_0 &= -\frac{2}{\pi}\sqrt{(PQ)} \\ \Psi_1 - X\Psi_0 &= \frac{1}{3\pi}[P+Q]\sqrt{(PQ)} \\ \Psi_2 - 2X\Psi_1 + X^2\Psi_0 &= -\frac{1}{\pi}\left[\frac{1}{10}P^2 + \frac{1}{9}PQ + \frac{1}{10}Q^2\right]\sqrt{(PQ)} \end{aligned}\right\},$$

where the definition of the parameters (P, Q) in terms of the non-dimensional co-ordinates (X, Y) is dependent on the region J.

Region B

$$F_{mB}(X, Y) = \Psi_m(P, Q),$$

where

$$\left.\begin{aligned} P &= X - Y \\ Q &= X + Y \end{aligned}\right\}.$$

Region F

$$F_{mF}(X, Y) = \Psi_m(P, Q),$$

where

$$\left.\begin{aligned} P &= 2\left(\frac{\tau X_2 - Y_2}{\tau + 1}\right) \\ Q &= X_2 + Y_2 \end{aligned}\right\}$$

and

$$X_2 = X + \delta Y_L, \quad Y_2 = Y - \delta Y_L.$$

Region H

$$F_{mH}(X, Y) = F_{mF}(X, Y) + F_{mF}(X, -Y) - F_{mB}(X, Y).$$

APPENDIX D

Estimation of Thickness Corrections by Strip Theory

In the main body of this report, the lift and pitching-moment derivatives have been evaluated on the assumption that the wings are of zero thickness. The models used in the N.P.L. experiments had finite thickness as defined in Section 6.2, and it is desirable to estimate its effect on the derivatives.

Van Dyke[5] has derived a solution for the loading on two-dimensional aerofoils of small finite thickness oscillating in supersonic flow. For slow oscillations of a symmetrical profile, the contribution made by the thickness to the lift distribution over the aerofoil surface is

$$\Delta l = 2\rho_\infty U_\infty{}^2\theta_0 e^{i\omega t}\left\{\frac{(M^2N-2)}{\beta^2}Z' - \frac{i\omega}{U_\infty}\left[\frac{2M^2(N-1)}{\beta^4}Z + \right.\right.$$
$$\left.\left. + \frac{(2-M^2)(M^2N-1)}{\beta^4}xZ' + \frac{(M^2N-2)}{\beta^2}hcZ'\right]\right\}, \quad \text{(D.1)}$$

where $z = \pm Z(x)$, $(0 \leqslant x \leqslant c)$, is the equation of the symmetrical aerofoil,

hc is the distance of the pitching axis downstream of the leading edge

$N = (\gamma+1)M^2/2\beta^2 = 1 \cdot 2M^2/\beta^2$ for air,

and $Z' = dZ/dx$.

Eqn. (D.1) applies to aerofoils having an attached shock wave at the nose; the leading edge must therefore be sharp, though the trailing edge may be blunt.

To estimate the effect of thickness on the three-dimensional wings, the above equation was applied on the basis of simple strip theory. If the pitching axis is at a distance h_0c_0 downstream of the wing apex (Fig. 1) and the equation of the leading edge of the wing is $x = x_l(y)$, the local pitching axis is defined by

$$h(y)\,c(y) = h_0 c_0 - x_l(y)\,. \tag{D.2}$$

Then the thickness correction to the total lift on the wing is

$$\Delta L = \int_{y=-s}^{s} \int_{x=x_l(y)}^{x_l(y)+c(y)} \Delta l\, dx\, dy\,, \tag{D.3}$$

and the increment to the total pitching moment about the axis $x = h_0 c_0$ is

$$\Delta \mathscr{M} = -\int_{y=-s}^{s} \int_{x=x_l(y)}^{x_l(y)+c(y)} (x - h_0 c_0)\Delta l\, dx\, dy\,, \tag{D.4}$$

where $\Delta l(x, y, t)$ is given by eqn. (D.1) with x and hc replaced by $\{x - x_l(y)\}$ and $\{h_0 c_0 - x_l(y)\}$ respectively, since these are now the distances of the point (x, y) and the local pitching axis from the leading edge.

When the streamwise aerofoil section is a symmetrical double-wedge with thickness/chord ratio equal to δ, the integration of eqns. (D.3) and (D.4) in the chordwise direction is particularly simple. With $Z = \frac{1}{2}\delta\{c - |c - 2(x - x_l)|\}$, $(x_l \leqslant x \leqslant x_l + c)$,
it follows that

$$\Delta \text{ (Local lift per unit span)} = -\tfrac{1}{2}\rho_\infty U_\infty{}^2 \theta_0 e^{i\omega t} c\delta \left[\frac{i\omega c}{U_\infty}\left(\frac{M^4 N - 3M^2 + 2}{\beta^4}\right)\right], \tag{D.5}$$

and

Δ (Local pitching moment per unit span about axis $h_0 c_0$)

$$= \tfrac{1}{2}\rho_\infty U_\infty{}^2 \theta_0 e^{i\omega t} c^2 \delta \left\{\left(\frac{M^2 N - 2}{\beta^2}\right) + \frac{i\omega c}{U_\infty}\left[\left(\frac{M^2 N - 2}{\beta^2}\right)(1 - 2h) - \frac{M^2(N-1)}{\beta^4} h\right]\right\}, \tag{D.6}$$

where h is defined by (D.2). Hence for a three-dimensional wing having a double-wedge section of constant ratio δ across the whole span, the total forces of eqns. (D.3) and (D.4) can easily be obtained by integrating (D.5) and (D.6) across the span. Then, the increments to the lift and pitching-moment derivatives as defined in eqn. (28) are found to be

$$\left.\begin{aligned}
\Delta l_\theta &= 0 \\
\Delta l_{\dot\theta} &= -\delta\left(\frac{c_0}{S}\right)\left(\frac{M^4 N - 3M^2 + 2}{\beta^4}\right)\int_0^s \left(\frac{c}{c_0}\right)^2 dy \\
\Delta m_\theta &= \delta\left(\frac{c_0}{S}\right)\left(\frac{M^2 N - 2}{\beta^2}\right)\int_0^s \left(\frac{c}{c_0}\right)^2 dy \\
\Delta m_{\dot\theta} &= \delta\left(\frac{c_0}{S}\right)\left[\left(\frac{M^2 N - 2}{\beta^2}\right)\int_0^s \left(\frac{c}{c_0}\right)^3 dy + P\int_0^s \frac{x_l}{c_0}\left(\frac{c}{c_0}\right)^2 dy - h_0 P \int_0^s \left(\frac{c}{c_0}\right)^2 dy\right]
\end{aligned}\right\}, \tag{D.7}$$

where

$$P = \frac{2(M^2 N - 2)}{\beta^2} + \frac{M^2(N-1)}{\beta^4}$$

and

$$N = 1 \cdot 2M^2/\beta^2\,.$$

The wings with blunt trailing side edges do not have a double-wedge section across the whole span (Section 6.2). To calculate the thickness corrections for these wings, the modified profile $Z(x)$ at the streamwise sections $s_T \leqslant |y| \leqslant s$ was used in eqns. (D.1) to (D.4).

TABLE 1

Regions of Integration for the Various Planforms and Mach Numbers

Planform	M	Case*	Regions J
$s = 1 \cdot 370 c_0$	$\sqrt{2}$	(i)	A, B
$\psi = -45°$	$1 \cdot 6$	(i)	A, B
	$1 \cdot 8$	(i)	A, B
	$2 \cdot 0$	(i)	A, B
	$2 \cdot 2$	(i)	A, B
	$2 \cdot 4$	(i)	A, B
$s = 1 \cdot 370 c_0$	$\sqrt{2}$	(ii)	as for
$\psi = -30°$	$1 \cdot 6$	(ii)	$s = 1 \cdot 370 c_0$
	$1 \cdot 8$	(ii)	$\psi = 30°$
	$2 \cdot 0$	(i)	A, B
	$2 \cdot 2$	(i)	A, B
	$2 \cdot 4$	(i)	A, B
$s = 1 \cdot 370 c_0$	$1 \cdot 035$	(iii)	B, F, H
$\psi = 0$	$1 \cdot 065$	(iii)	A, B, C, D, E, F, G
	$1 \cdot 102$	(iii)	A, B, C, D
	$1 \cdot 155$	(iii)	A, B, C, D
	$\sqrt{2}$	(iii)	A, B, C
	$1 \cdot 6$	(iii)	A, B, C
	$1 \cdot 8$	(iii)	A, B, C
	$2 \cdot 0$	(iii)	A, B, C
	$2 \cdot 2$	(iii)	A, B, C
	$2 \cdot 4$	(iii)	A, B, C
$s = 1 \cdot 370 c_0$	$\sqrt{2}$	(iv)	A, B, C, D
$\psi = 30°$	$1 \cdot 6$	(iv)	A, B, C
	$1 \cdot 8$	(iv)	A, B, C
	$2 \cdot 0$	(v)	as for
	$2 \cdot 2$	(v)	$s = 1 \cdot 370 c_0$
	$2 \cdot 4$	(v)	$= -30°$
$s = 1 \cdot 370 c_0$	$1 \cdot 155$	(iv)	A, B, C, D, E
$\psi = 45°$	$\sqrt{2}$	(v)	as for
	$1 \cdot 6$	(v)	$s = 1 \cdot 370 c_0$
	$1 \cdot 8$	(v)	$\psi = -45°$
	$2 \cdot 0$	(v)	
	$2 \cdot 2$	(v)	
	$2 \cdot 4$	(v)	

* Cases (i) to (v) are defined in Section 2.3.

TABLE 1—*continued*

Planform	M	Case*	Regions J
$s = 1\cdot000c_0$ $\psi = -30°$	$\sqrt{2}$	(ii)	as for $s = 1\cdot000c_0$ $\psi = 30°$
	$1\cdot6$	(ii)	
	$1\cdot8$	(ii)	
	$2\cdot0$	(i)	A, B
	$2\cdot2$	(i)	A, B
	$2\cdot4$	(i)	A, B
$s = 1\cdot000c_0$ $\psi = 0$	$\sqrt{2}$	(iii)	A, B, C, D
	$1\cdot6$	(iii)	A, B, C, D
	$1\cdot8$	(iii)	A, B, C
	$2\cdot0$	(iii)	A, B, C
	$2\cdot2$	(iii)	A, B, C
	$2\cdot4$	(iii)	A, B, C
$s = 1\cdot000c_0$ $\psi = 30°$	$\sqrt{2}$	(iv)	A, B, C, D, E
	$1\cdot6$	(iv)	A, B, C, D
	$1\cdot8$	(iv)	A, B, C, D
	$2\cdot0$	(v)	as for $s = 1\cdot000c_0$ $\psi = -30°$
	$2\cdot2$	(v)	
	$2\cdot4$	(v)	
$s = 0\cdot625c_0$ $\psi = -15°$	$\sqrt{2}$	(ii)	as for $s = 0\cdot625c_0$ $\psi = 15°$
	$1\cdot6$	(ii)	
	$1\cdot8$	(ii)	
	$2\cdot0$	(ii)	
	$2\cdot2$	(ii)	
	$2\cdot4$	(ii)	
$s = 0\cdot625c_0$ $\psi = 0$	$\sqrt{2}$	(iii)	A, B, C, D, E, F
	$1\cdot6$	(iii)	A, B, C, D, E, F
	$1\cdot8$	(iii)	A, B, C, D
	$2\cdot0$	(iii)	A, B, C, D
	$2\cdot2$	(iii)	A, B, C, D
	$2\cdot4$	(iii)	A, B, C, D
$s = 0\cdot625c_0$ $\psi = 15°$	$\sqrt{2}$	(iv)	A, B, C, D, E, F, G
	$1\cdot6$	(iv)	A, B, C, D, E, F
	$1\cdot8$	(iv)	A, B, C, D, E
	$2\cdot0$	(iv)	A, B, C, D, E
	$2\cdot2$	(iv)	A, B, C, D, E
	$2\cdot4$	(iv)	A, B, C, D

* Cases (i) to (v) are defined in Section 2.3.

TABLE 2

Stability Derivatives for Wings $s = 1\cdot37c_0$ with Pitching Axis $h_0 = 0$

ψ	M	l_θ	$l_{\dot\theta}$	$-m_\theta$	$-m_{\dot\theta}$
$-45°$	$\sqrt{2}$	1·9349	0·3458	0·9432	0·1921
	1·6	1·5658	0·4555	0·7670	0·2615
	1·8	1·3148	0·4636	0·6459	0·2689
	2·0	1·1404	0·4432	0·5613	0·2583
	2·2	1·0105	0·4163	0·4980	0·2433
	2·4	0·9093	0·3893	0·4485	0·2279
$-30°$	$\sqrt{2}$	1·9109	0·3483	0·9349	0·1940
	1·6	1·5567	0·4582	0·7663	0·2634
	1·8	1·3124	0·4668	0·6484	0·2711
	2·0	1·1412	0·4468	0·5651	0·2607
	2·2	1·0111	0·4194	0·5012	0·2454
	2·4	0·9097	0·3920	0·4513	0·2298
0	1·035	4·1077	−9·2227	1·5419	−3·8874
	1·064	3·8766	−5·5442	1·6754	−2·9333
	1·102	3·5173	−3·0357	1·6295	−1·7608
	1·155	3·0271	−1·2496	1·4441	−0·7551
	$\sqrt{2}$	1·8928	+0·3518	0·9290	+0·1961
	1·6	1·5396	+0·4590	0·7599	+0·2639
	1·8	1·2967	+0·4662	0·6421	+0·2706
	2·0	1·1270	+0·4455	0·5592	+0·2598
	2·2	1·0001	+0·4184	0·4969	+0·2447
	2·4	0·9008	+0·3912	0·4481	+0·2292
30°	$\sqrt{2}$	1·9109	0·3549	0·9415	0·2004
	1·6	1·5567	0·4634	0·7715	0·2686
	1·8	1·3124	0·4711	0·6526	0·2753
	2·0	1·1412	0·4504	0·5687	0·2643
	2·2	1·0111	0·4227	0·5045	0·2487
	2·4	0·9097	0·3950	0·4544	0·2327
45°	1·155	3·0452	−1·1841	1·4591	−0·6920
	$\sqrt{2}$	1·9349	+0·3611	0·9585	+0·2071
	1·6	1·5658	+0·4687	0·7801	+0·2743
	1·8	1·3148	+0·4749	0·6572	+0·2799
	2·0	1·1404	+0·4532	0·5712	+0·2680
	2·2	1·0105	+0·4252	0·5069	+0·2520
	2·4	0·9093	+0·3973	0·4565	+0·2358

TABLE 3

Stability Derivatives for Wings $s = 1 \cdot 00c_0$ with Pitching Axis $h_0 = 0$

ψ	M	l_θ	$l_{\dot{\theta}}$	$-m_\theta$	$-m_{\dot{\theta}}$
$-30°$	$\sqrt{2}$	1·7922	0·3426	0·8364	0·2025
	1·6	1·5041	0·4352	0·7158	0·2564
	1·8	1·2898	0·4457	0·6203	0·2635
	2·0	1·1335	0·4297	0·5484	0·2547
	2·2	1·0057	0·4051	0·4874	0·2406
	2·4	0·9057	0·3797	0·4395	0·2258
0	$\sqrt{2}$	1·7380	0·3451	0·8311	0·2047
	1·6	1·4475	0·4418	0·7024	0·2625
	1·8	1·2357	0·4509	0·6043	0·2689
	2·0	1·0829	0·4332	0·5321	0·2588
	2·2	0·9665	0·4085	0·4763	0·2445
	2·4	0·8742	0·3832	0·4318	0·2296
30°	$\sqrt{2}$	1·7922	0·3879	0·8817	0·2453
	1·6	1·5041	0·4707	0·7514	0·2906
	1·8	1·2898	0·4750	0·6495	0·2921
	2·0	1·1335	0·4547	0·5735	0·2794
	2·2	1·0057	0·4277	0·5100	0·2629
	2·4	0·9057	0·4003	0·4601	0·2461

TABLE 4

Stability Derivatives for Wings $s = 0 \cdot 625c_0$ with Pitching Axis $h_0 = 0$

ψ	M	l_θ	$l_{\dot\theta}$	$-m_\theta$	$-m_{\dot\theta}$
$-15°$	$\sqrt{2}$	1·3830	0·5026	0·5495	0·3401
	1·6	1·2471	0·4842	0·5339	0·3076
	1·8	1·1187	0·4561	0·4986	0·2832
	2·0	1·0112	0·4265	0·4609	0·2626
	2·2	0·9218	0·3979	0·4262	0·2441
	2·4	0·8468	0·3717	0·3954	0·2275
0	$\sqrt{2}$	1·3483	0·5142	0·5688	0·3498
	1·6	1·2065	0·4965	0·5409	0·3194
	1·8	1·0762	0·4678	0·4985	0·2947
	2·0	0·9677	0·4376	0·4562	0·2736
	2·2	0·8787	0·4082	0·4187	0·2544
	2·4	0·8047	0·3811	0·3864	0·2371
15°	$\sqrt{2}$	1·3830	0·5835	0·6303	0·4038
	1·6	1·2471	0·5447	0·5944	0·3619
	1·8	1·1187	0·5047	0·5472	0·3292
	2·0	1·0112	0·4679	0·5022	0·3025
	2·2	0·9218	0·4342	0·4625	0·2794
	2·4	0·8468	0·4040	0·4278	0·2593

TABLE 5

Thickness Corrections for Wings $s = 1 \cdot 37 c_0$ with Pitching Axis $h_0 = 0$

Section	ψ	M	Δl_θ	$\Delta l_{\dot\theta}$	$-\Delta m_\theta$	$-\Delta m_{\dot\theta}$
a	$-45°$	$\sqrt{2}$	0·010	−0·098	−0·045	−0·055
		1·6	0·007	−0·051	−0·032	−0·036
		1·8	0·006	−0·035	−0·026	−0·029
		2·0	0·005	−0·029	−0·024	−0·026
		2·2	0·005	−0·026	−0·022	−0·024
		2·4	0·005	−0·024	−0·022	−0·023
a	$-30°$	$\sqrt{2}$	0·005	−0·098	−0·048	−0·055
		1·6	0·003	−0·052	−0·033	−0·036
		1·8	0·003	−0·036	−0·028	−0·029
		2·0	0·002	−0·030	−0·025	−0·026
		2·2	0·002	−0·027	−0·024	−0·025
		2·4	0·002	−0·025	−0·023	−0·024
b	0	$\sqrt{2}$	0	−0·099	−0·049	−0·055
		1·6	0	−0·052	−0·034	−0·036
		1·8	0	−0·037	−0·028	−0·029
		2·0	0	−0·031	−0·026	−0·026
		2·2	0	−0·027	−0·024	−0·025
		2·4	0	−0·026	−0·024	−0·024
c	30°	$\sqrt{2}$	0	−0·100	−0·050	−0·056
		1·6	0	−0·053	−0·035	−0·037
		1·8	0	−0·037	−0·029	−0·030
		2·0	0	−0·031	−0·026	−0·027
		2·2	0	−0·028	−0·025	−0·025
		2·4	0	−0·026	−0·024	−0·024
c	45°	$\sqrt{2}$	0	−0·100	−0·050	−0·056
		1·6	0	−0·053	−0·035	−0·037
		1·8	0	−0·038	−0·029	−0·030
		2·0	0	−0·031	−0·026	−0·027
		2·2	0	−0·028	−0·025	−0·025
		2·4	0	−0·026	−0·024	−0·024

a Blunt trailing side-edges (*see* Section 6.2).

b 5% double-wedge section.

c Sharp leading side-edges (5% double-wedge section).

(86178) C

TABLE 6

Thickness Corrections for Wings $s = 1 \cdot 00 c_0$ with Pitching Axis $h_0 = 0$

Section	ψ	M	Δl_θ	$\Delta l_{\dot{\theta}}$	$-\Delta m_\theta$	$-\Delta m_{\dot{\theta}}$
a	$-30°$	$\sqrt{2}$	0·018	−0·108	−0·046	−0·058
		1·6	0·013	−0·055	−0·032	−0·038
		1·8	0·010	−0·037	−0·027	−0·030
		2·0	0·009	−0·030	−0·024	−0·027
		2·2	0·009	−0·027	−0·023	−0·025
		2·4	0·009	−0·025	−0·022	−0·024
b	0	$\sqrt{2}$	0	−0·107	−0·054	−0·059
		1·6	0	−0·057	−0·037	−0·039
		1·8	0	−0·040	−0·031	−0·032
		2·0	0	−0·033	−0·028	−0·029
		2·2	0	−0·030	−0·026	−0·027
		2·4	0	−0·028	−0·026	−0·026
c	30°	$\sqrt{2}$	0	−0·108	−0·054	−0·060
		1·6	0	−0·057	−0·037	−0·040
		1·8	0	−0·040	−0·031	−0·032
		2·0	0	−0·033	−0·028	−0·029
		2·2	0	−0·030	−0·027	−0·027
		2·4	0	−0·028	−0·026	−0·026

a Blunt trailing side-edges (*see* Section 6.2).

b 5% double-wedge section.

c Sharp leading side-edges (5% double-wedge section).

TABLE 7

Thickness Corrections for Wings $s = 0 \cdot 625 c_0$ with Pitching Axis $h_0 = 0$

Section	ψ	M	Δl_θ	$\Delta l_{\dot\theta}$	$-\Delta m_\theta$	$-\Delta m_{\dot\theta}$
a	$-15°$	$\sqrt{2}$	0·021	−0·120	−0·050	−0·062
		1·6	0·015	−0·060	−0·035	−0·040
		1·8	0·012	−0·041	−0·029	−0·032
		2·0	0·011	−0·033	−0·026	−0·029
		2·2	0·010	−0·029	−0·025	−0·027
		2·4	0·010	−0·027	−0·024	−0·026
b	0	$\sqrt{2}$	0	−0·118	−0·059	−0·063
		1·6	0	−0·063	−0·041	−0·043
		1·8	0	−0·044	−0·034	−0·035
		2·0	0	−0·037	−0·031	−0·031
		2·2	0	−0·033	−0·029	−0·029
		2·4	0	−0·031	−0·028	−0·028
c	15°	$\sqrt{2}$	0	−0·116	−0·058	−0·063
		1·6	0	−0·061	−0·040	−0·043
		1·8	0	−0·043	−0·033	−0·035
		2·0	0	−0·036	−0·030	−0·031
		2·2	0	−0·032	−0·029	−0·029
		2·4	0	−0·030	−0·028	−0·028

a Blunt trailing side-edges (*see* Section 6.2).

b 5% double-wedge section.

c Sharp leading side-edges (5% double-wedge section).

TABLE 8

Conversion Factors for Derivatives [see Eqns. (48) *and* (49)]

s/c_0	$\|\psi\|$	Aspect ratio	$c_0/\bar{c}$	$(c_0/\bar{c})^2$	$c_0/\bar{\bar{c}}$	$(c_0/\bar{\bar{c}})^2$
1·370	45°	4·5844	1·67313	2·79936	1·39503	1·94610
	30°	4·4531	1·62523	2·64139	1·40444	1·97245
	0	4·3292	1·58000	2·49641	1·42070	2·01837
1·000	30°	3·0372	1·51862	2·30620	1·30141	1·69368
	0	2·7321	1·36603	1·86603	1·30763	1·70989
0·625	15°	1·7114	1·36914	1·87455	1·20750	1·45806
	0	1·5014	1·20116	1·44277	1·18517	1·40463

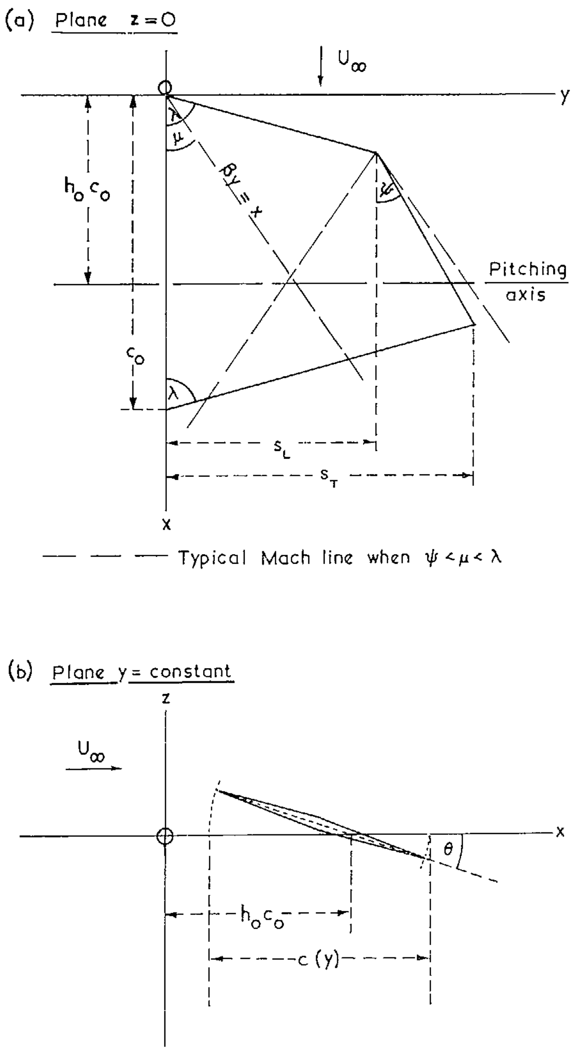

Instantaneous incidence $\theta = \theta_0 \cos \omega t$.

5% thick double-wedge section extends to $y = s_L$ for $\psi > 0$.

FIGS. 1a and b. Planform and streamwise section of half-wing.

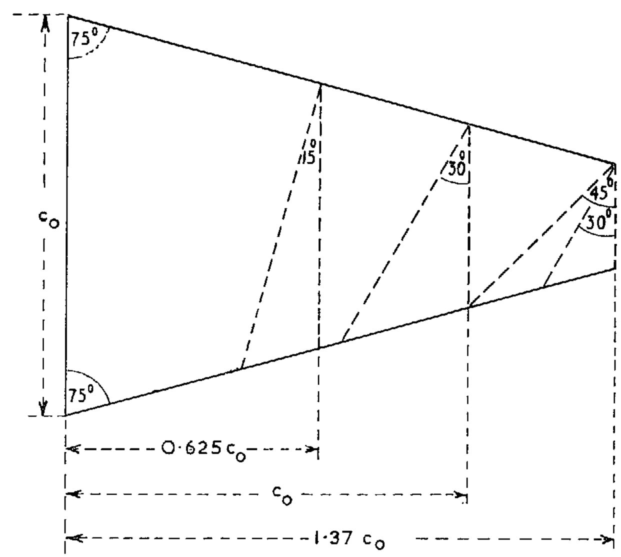

$\lambda = 75°$	s/c_0	0·625	0·625	1·000	1·000	1·370	1·370	1·370
	ψ	±15°	0	±30°	0	±45°	±30°	0

FIG. 2. Definition of family of wings.

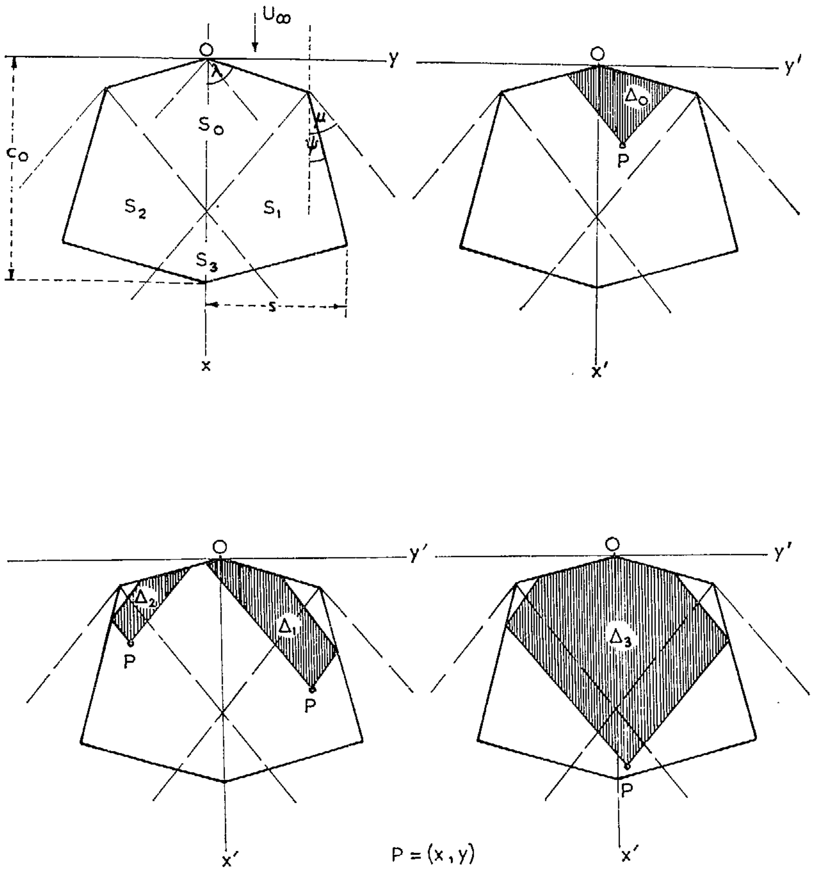

FIG. 3. Regions of planform and areas of integration in equation (13).

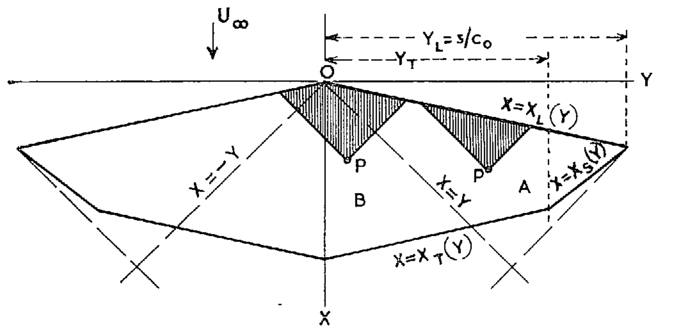

Shaded areas show Δ_A and Δ_B for $P = (X, Y)$ in regions A and B.

(a) Case (i) with supersonic trailing side-edges:
$\lambda = 75°$, $s = 1{\cdot}370\ c_0$, $\psi = -45°$, $M = 1{\cdot}6$

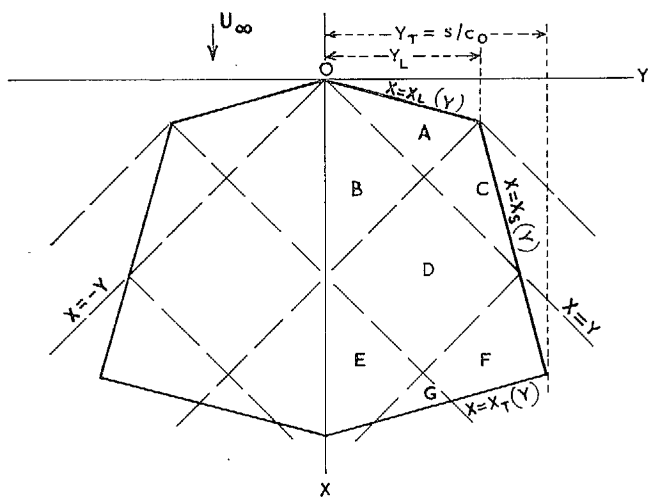

(b) Case (iv) with subsonic leading side-edges:
$\lambda = 75°$, $s = 0{\cdot}625\ c_0$, $\psi = 15°$, $M = \sqrt{2}$

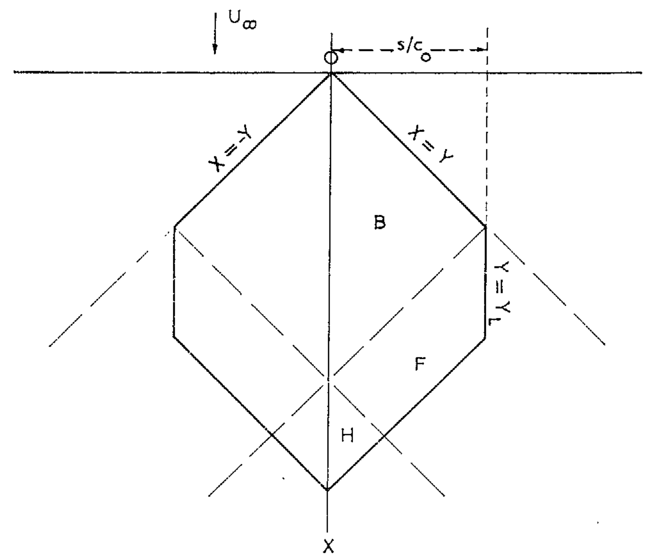

(c) Case (iii) with sonic leading and trailing edges:
$\lambda = 75°$, $s = 1{\cdot}370\ c_0$, $\psi = 0$, $M = 1{\cdot}035$

FIGS. 4a, b and c. Regions of typical planforms in the (X, Y) plane.

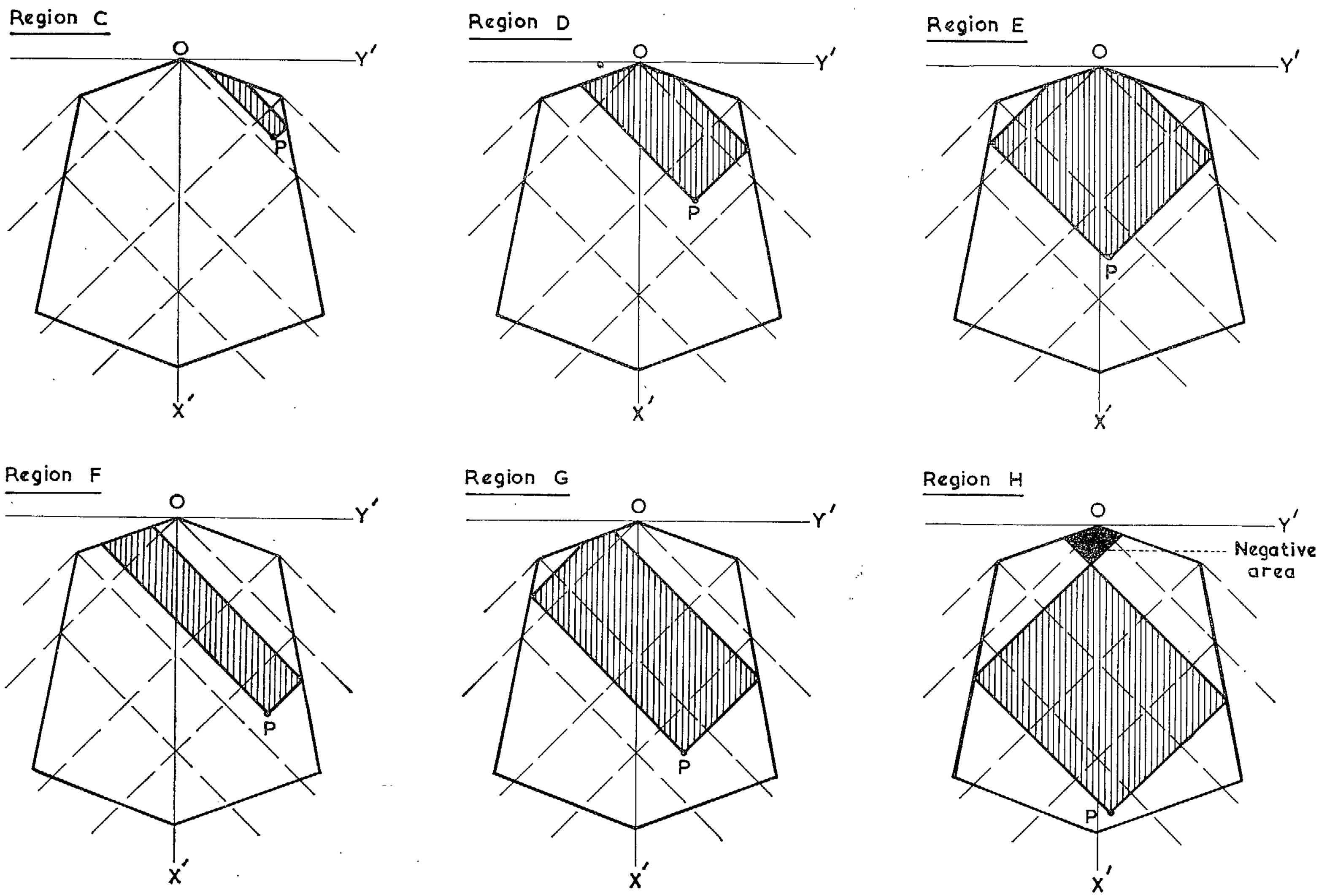

FIG. 5. Areas of integration Δ_J for P = (X, Y) in each region J = C, . . . H, of the planform with subsonic leading side-edges.

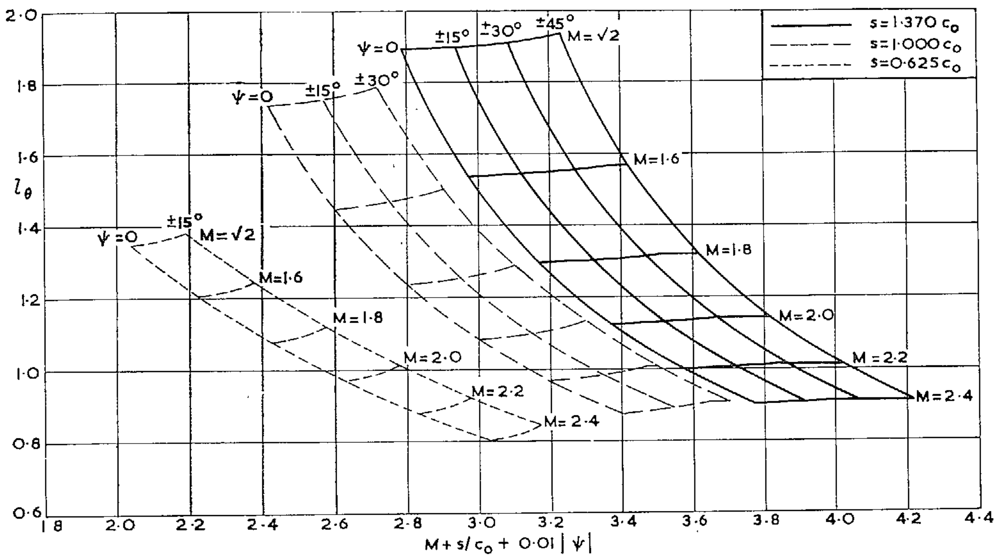

FIG. 6. Variation of l_θ with planform and Mach number.

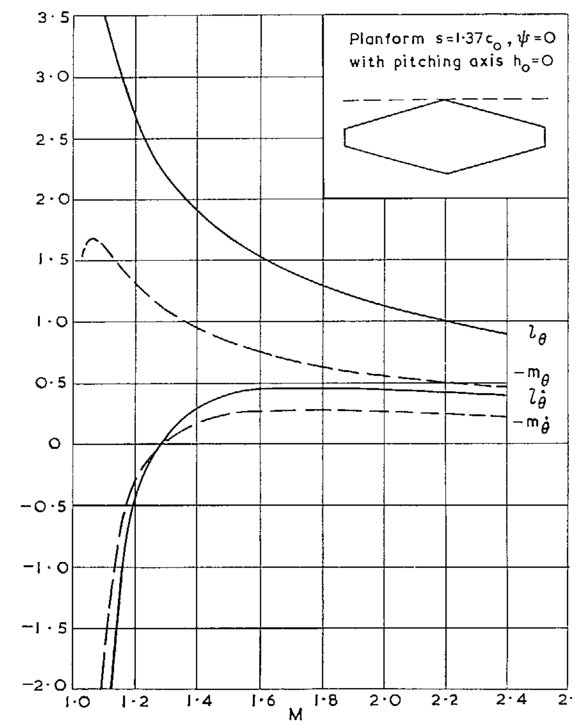

FIG. 7. Pitching derivatives against Mach number for wing with streamwise tips.

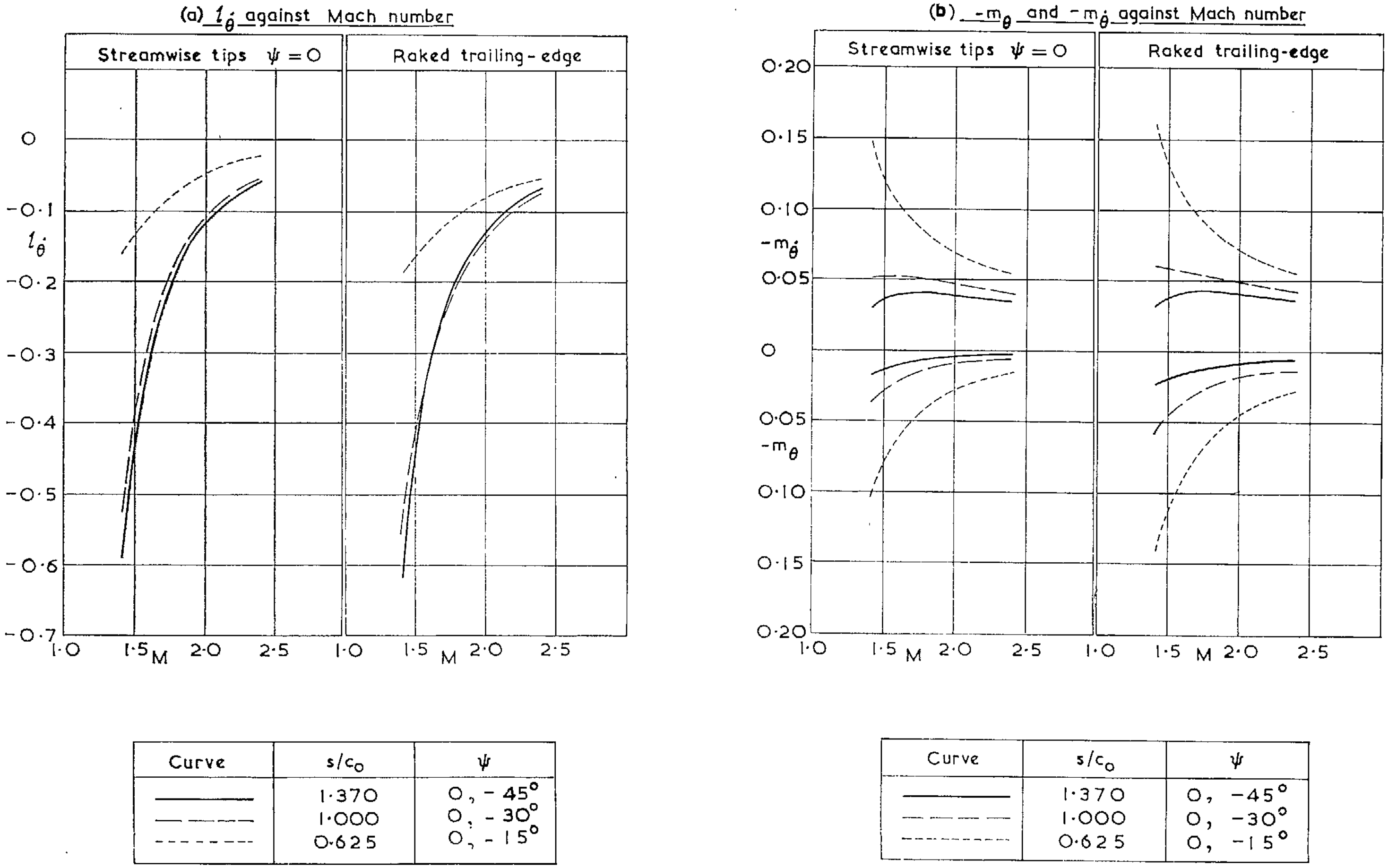

FIGS. 8a and b. Effects of span and raked trailing edge on derivatives for mid-chord pitching axis $h_0 = 0\cdot5$.

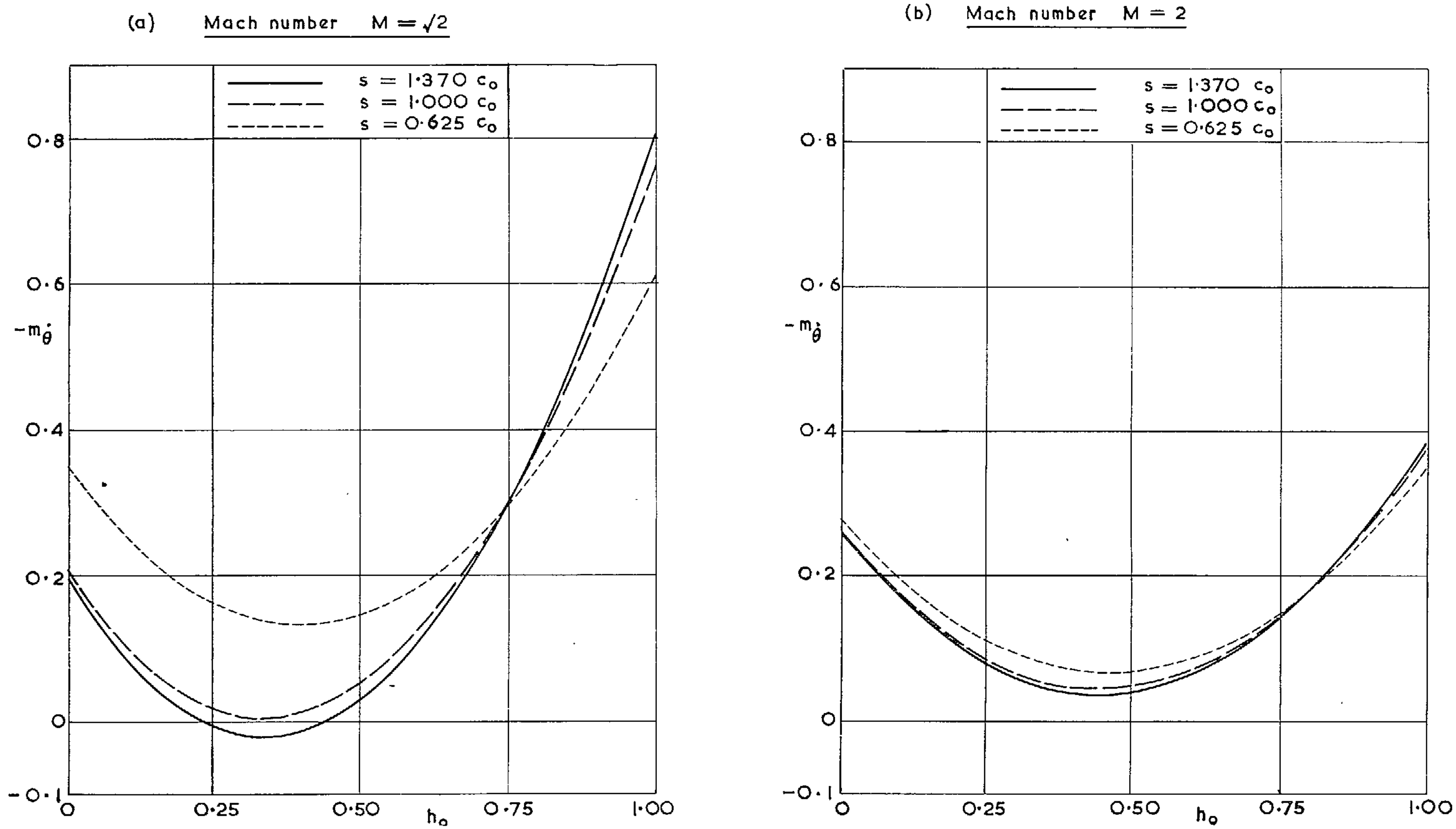

FIGS. 9a and b. Variation of $-m_{\dot\theta}$ with axis position h_0 for wings with streamwise tips.

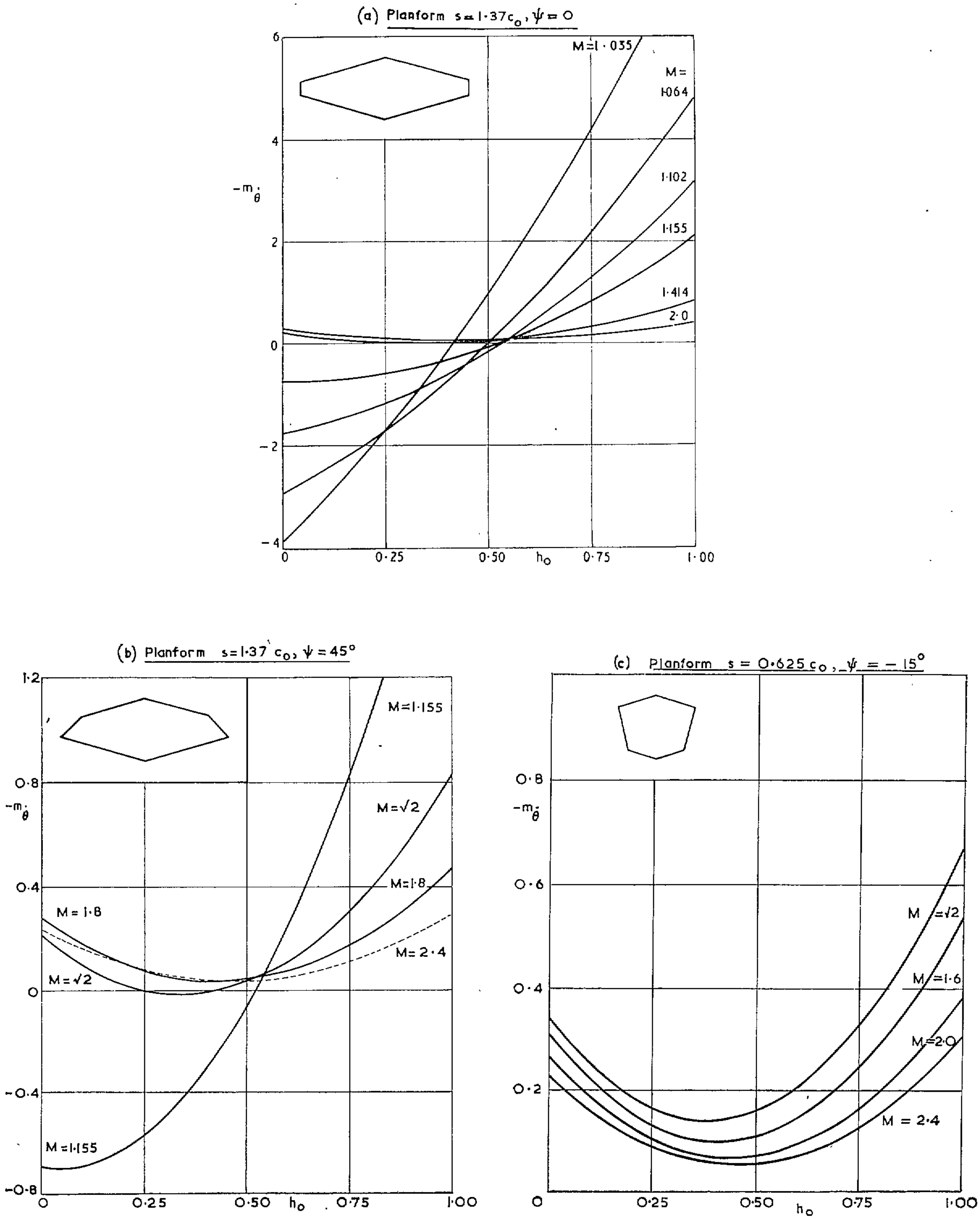

FIGS. 10a, b and c. Effect of Mach number on the pitching damping $-m_{\dot{\theta}}$ against h_0.

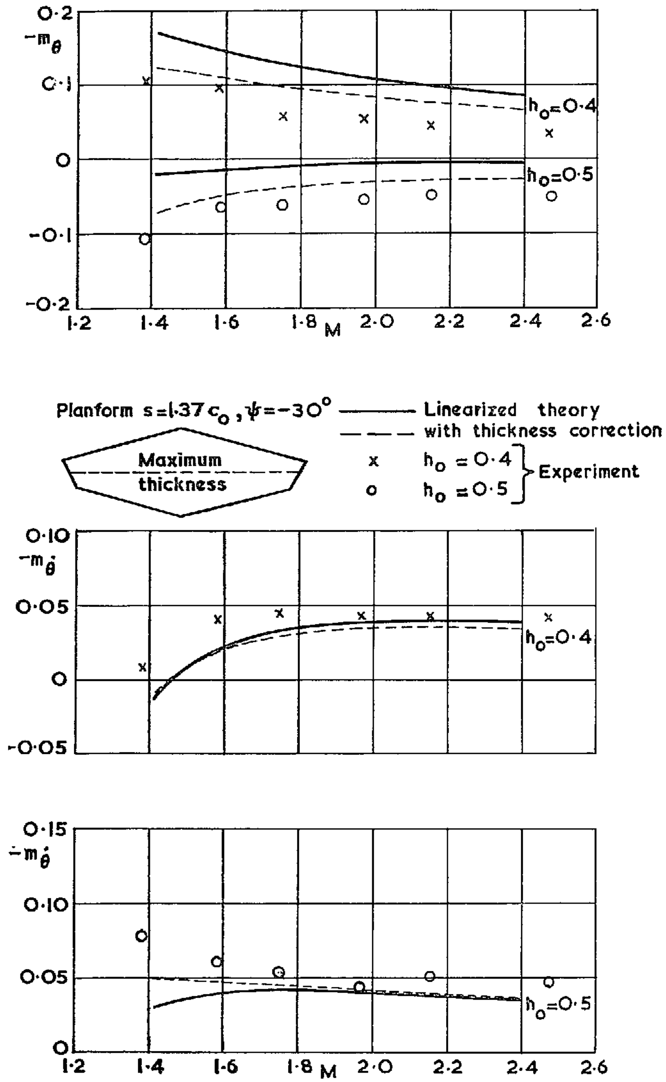

FIG. 11. Calculated and measured $-m_\theta$ and $-m_{\dot\theta}$ against M for wing with blunt trailing side edges.

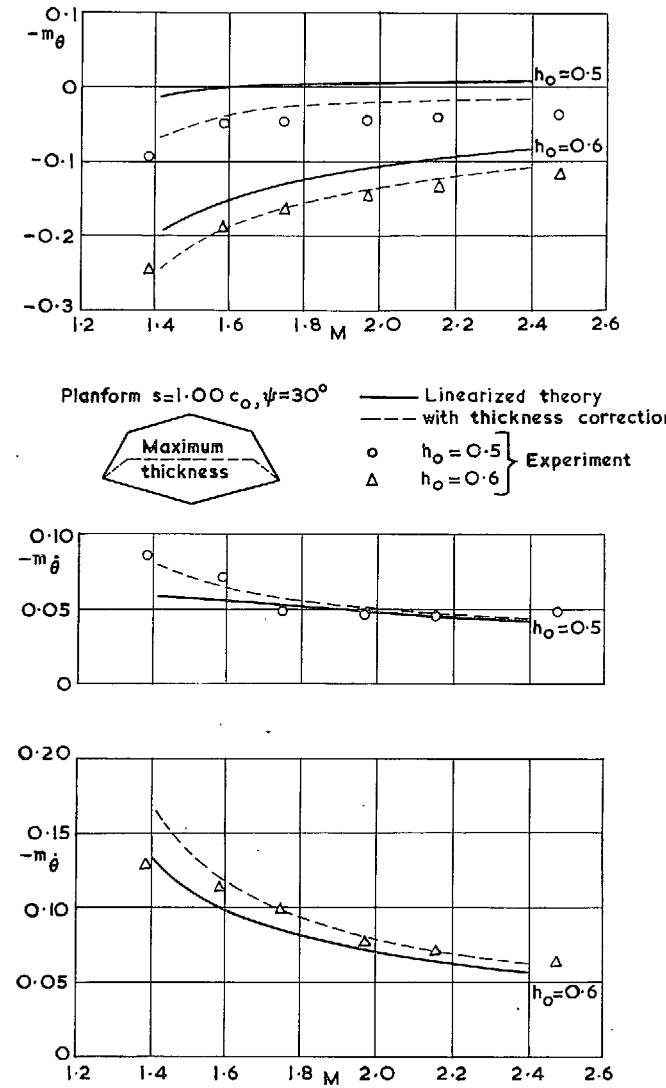

FIG. 12. Calculated and measured $-m_\theta$ and $-m_{\dot\theta}$ against M for wing with sharp leading side edges.

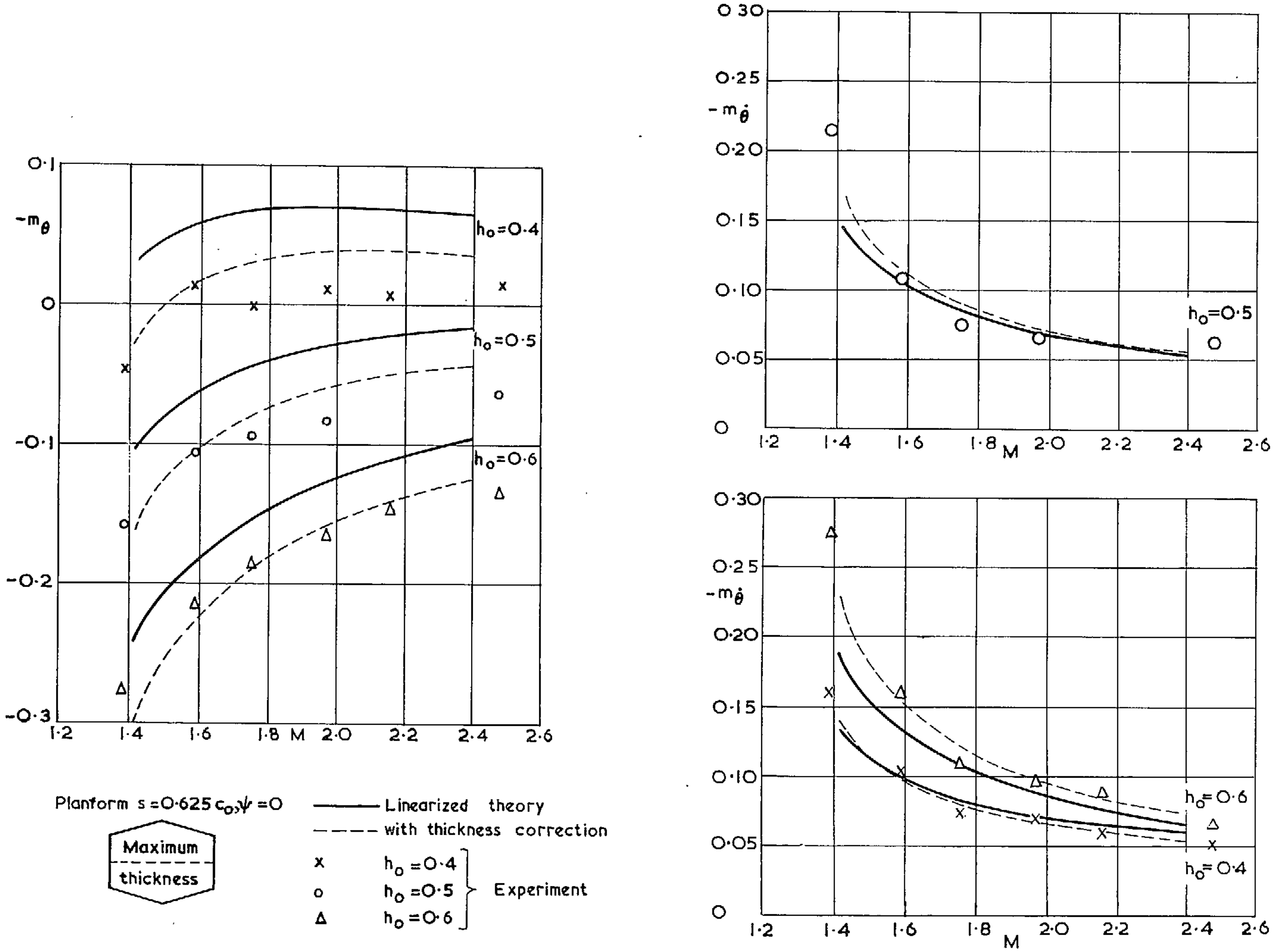

FIG. 13. Calculated and measured $-m_\theta$ and $-m_{\dot\theta}$ against M for wing with streamwise tips.

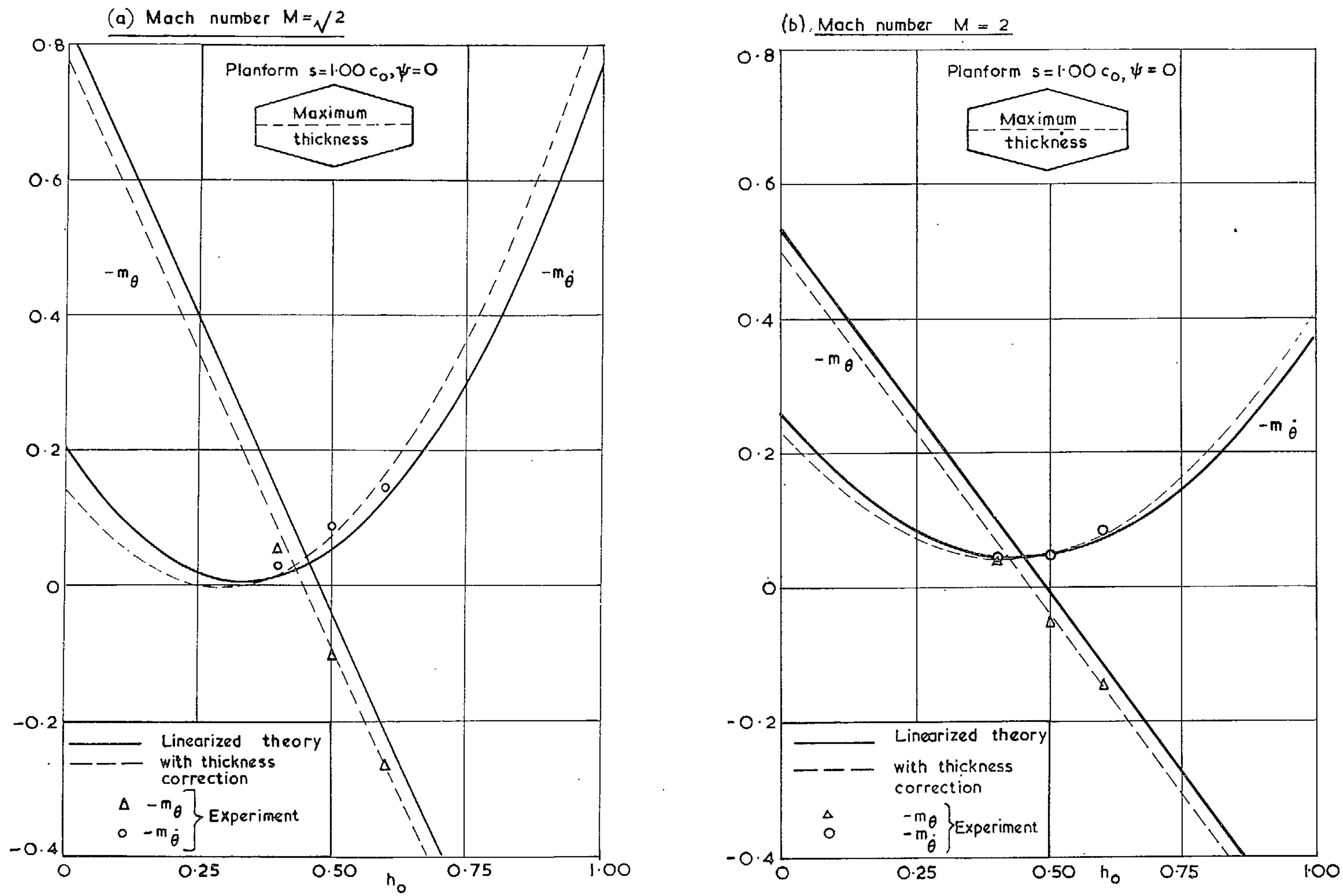

FIGS. 14a and b. Calculated and measured $-m_\theta$ and $-m_{\dot\theta}$ against h_0 for wing with streamwise tips.

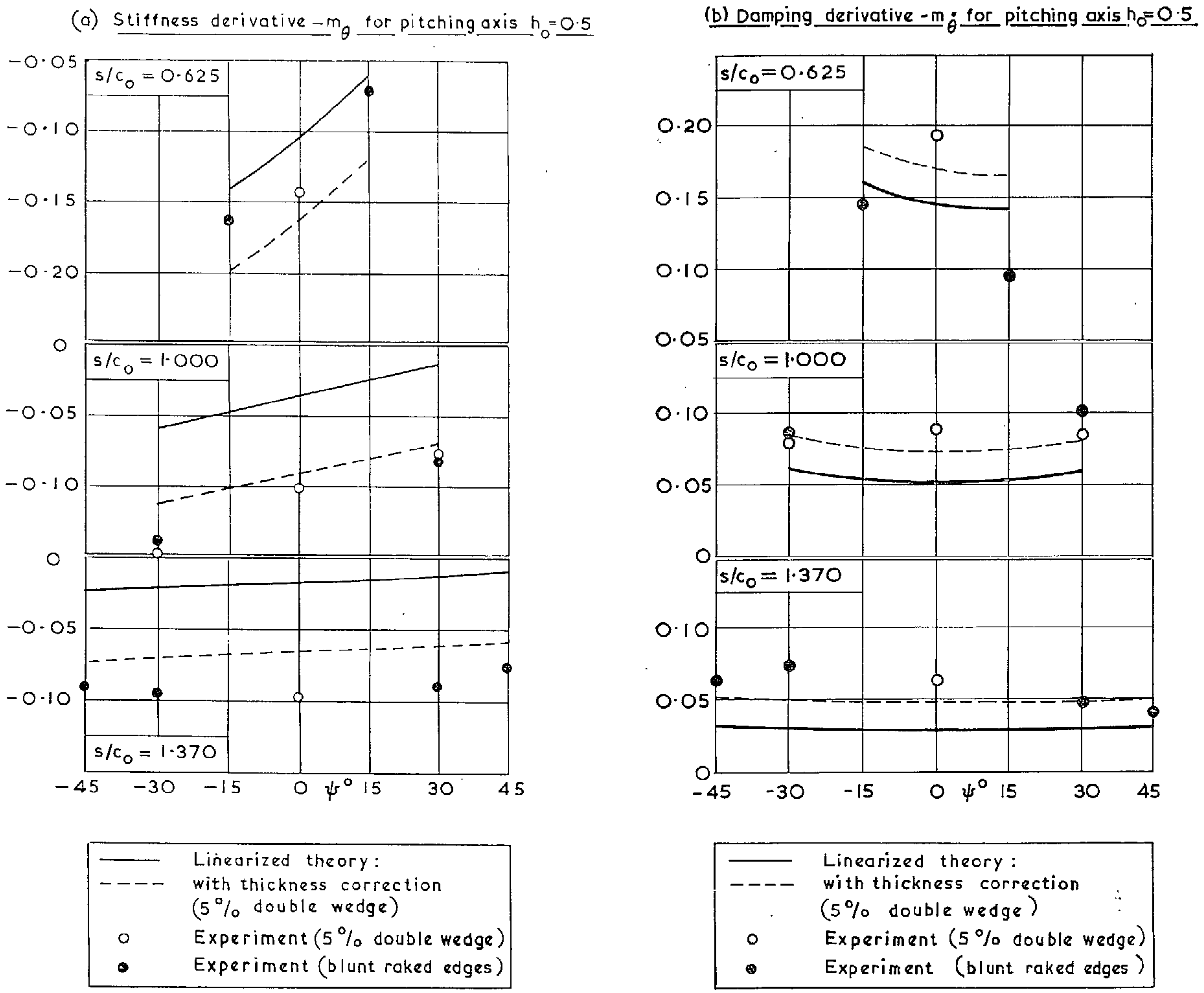

FIGS. 15a and b. Calculated and measured effect of side-edge rake for different spans of wing at $M = \sqrt{2}$.

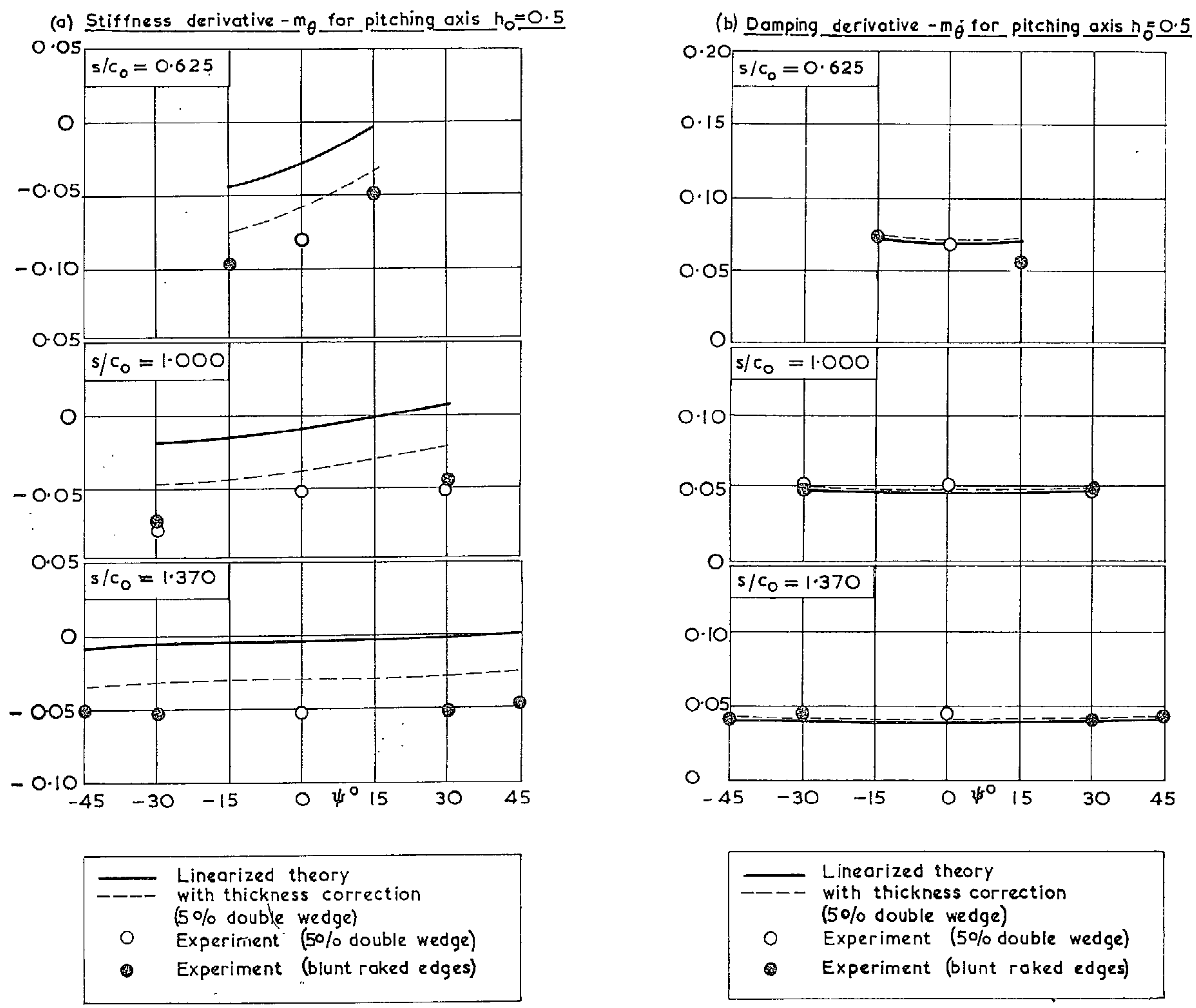

FIGS. 16a and b. Calculated and measured effect of side-edge rake for different spans of wing at $M = 2$.

(86178) Wt. 64/1857 K.5 3/63 Hw.

Publications of the Aeronautical Research Council

ANNUAL TECHNICAL REPORTS OF THE AERONAUTICAL RESEARCH COUNCIL (BOUND VOLUMES)

1942 Vol. I. Aero and Hydrodynamics, Aerofoils, Airscrews, Engines. 75*s.* (post 2*s.* 9*d.*)
Vol. II. Noise, Parachutes, Stability and Control, Structures, Vibration, Wind Tunnels. 47*s.* 6*d.* (post 2*s.* 3*d.*)

1943 Vol. I. Aerodynamics, Aerofoils, Airscrews. 80*s.* (post 2*s.* 6*d.*)
Vol. II. Engines, Flutter, Materials, Parachutes, Performance, Stability and Control, Structures. 90*s.* (post 2*s.* 9*d.*)

1944 Vol. I. Aero and Hydrodynamics, Aerofoils, Aircraft, Airscrews, Controls. 84*s.* (post 3*s.*)
Vol. II. Flutter and Vibration, Materials, Miscellaneous, Navigation, Parachutes, Performance, Plates and Panels, Stability, Structures, Test Equipment, Wind Tunnels. 84*s.* (post 3*s.*)

1945 Vol. I. Aero and Hydrodynamics, Aerofoils. 130*s.* (post 3*s.* 6*d.*)
Vol. II. Aircraft, Airscrews, Controls. 130*s.* (post 3*s.* 6*d.*)
Vol. III. Flutter and Vibration, Instruments, Miscellaneous, Parachutes, Plates and Panels, Propulsion. 130*s.* (post 3*s.* 3*d.*)
Vol. IV. Stability, Structures, Wind Tunnels, Wind Tunnel Technique. 130*s.* (post 3*s.* 3*d.*)

1946 Vol. I. Accidents, Aerodynamics, Aerofoils and Hydrofoils. 168*s.* (post 3*s.* 9*d.*)
Vol. II. Airscrews, Cabin Cooling, Chemical Hazards, Controls, Flames, Flutter, Helicopters, Instruments and Instrumentation, Interference, Jets, Miscellaneous, Parachutes. 168*s.* (post 3*s.* 3*d.*)
Vol. III. Performance, Propulsion, Seaplanes, Stability, Structures, Wind Tunnels. 168*s.* (post 3*s.* 6*d.*)

1947 Vol. I. Aerodynamics, Aerofoils, Aircraft. 168*s.* (post 3*s.* 9*d.*)
Vol. II. Airscrews and Rotors, Controls, Flutter, Materials, Miscellaneous, Parachutes, Propulsion, Seaplanes, Stability, Structures, Take-off and Landing. 168*s.* (post 3*s.* 9*d.*)

1948 Vol. I. Aerodynamics, Aerofoils, Aircraft, Airscrews, Controls, Flutter and Vibration, Helicopters, Instruments, Propulsion, Seaplane, Stability, Structures, Wind Tunnels. 130*s.* (post 3*s.* 3*d.*)
Vol. II. Aerodynamics, Aerofoils, Aircraft, Airscrews, Controls, Flutter and Vibration, Helicopters, Instruments, Propulsion, Seaplane, Stability, Structures, Wind Tunnels. 110*s.* (post 3*s.* 3*d.*)

Special Volumes

Vol. I. Aero and Hydrodynamics, Aerofoils, Controls, Flutter, Kites, Parachutes, Performance, Propulsion, Stability. 126*s.* (post 3*s.*)
Vol. II. Aero and Hydrodynamics, Aerofoils, Airscrews, Controls, Flutter, Materials, Miscellaneous, Parachutes, Propulsion, Stability, Structures. 147*s.* (post 3*s.*)
Vol. III. Aero and Hydrodynamics, Aerofoils, Airscrews, Controls, Flutter, Kites, Miscellaneous, Parachutes, Propulsion, Seaplanes, Stability, Structures, Test Equipment. 189*s.* (post 3*s.* 9*d.*)

Reviews of the Aeronautical Research Council

1939–48 3*s.* (post 6*d.*) 1949–54 5*s.* (post 5*d.*)

Index to all Reports and Memoranda published in the Annual Technical Reports

1909–1947 R. & M. 2600 (out of print)

Indexes to the Reports and Memoranda of the Aeronautical Research Council

Between Nos. 2351–2449	R. & M. No. 2450	2*s.* (post 3*d.*)
Between Nos. 2451–2549	R. & M. No. 2550	2*s.* 6*d.* (post 3*d.*)
Between Nos. 2551–2649	R. & M. No. 2650	2*s.* 6*d.* (post 3*d.*)
Between Nos. 2651–2749	R. & M. No. 2750	2*s.* 6*d.* (post 3*d.*)
Between Nos. 2751–2849	R. & M. No. 2850	2*s.* 6*d.* (post 3*d.*)
Between Nos. 2851–2949	R. & M. No. 2950	3*s.* (post 3*d.*)
Between Nos. 2951–3049	R. & M. No. 3050	3*s.* 6*d.* (post 3*d.*)
Between Nos. 3051–3149	R. & M. No. 3150	3*s.* 6*d.* (post 3*d.*)

HER MAJESTY'S STATIONERY OFFICE

from the addresses overleaf

Printed and published by
HER MAJESTY'S STATIONERY OFFICE

To be purchased from
York House, Kingsway, London W.C.2
423 Oxford Street, London W.1
13A Castle Street, Edinburgh 2
109 St. Mary Street, Cardiff
39 King Street, Manchester 2
50 Fairfax Street, Bristol 1
35 Smallbrook, Ringway, Birmingham 5
80 Chichester Street, Belfast 1
or through any bookseller

Printed in England

R. & M. No. 3298

S.O. Code No. 23-3298